



HAL
open science

The relationship between peak warming and cumulative CO₂ emissions, and its use to quantify vulnerabilities in the carbon-climate-human system

Michael Raupach, Josep Canadell, Philippe Ciais, Pierre Friedlingstein, Peter Rayner, Catherine Trudinger

► To cite this version:

Michael Raupach, Josep Canadell, Philippe Ciais, Pierre Friedlingstein, Peter Rayner, et al.. The relationship between peak warming and cumulative CO₂ emissions, and its use to quantify vulnerabilities in the carbon-climate-human system. *Tellus B - Chemical and Physical Meteorology*, 2011, 63 (2), pp.145-164. 10.1111/j.1600-0889.2010.00521.x . hal-02929059

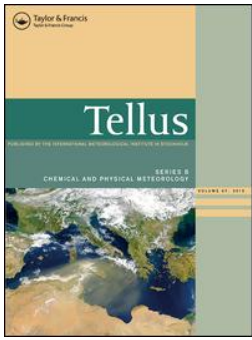
HAL Id: hal-02929059

<https://hal.science/hal-02929059>

Submitted on 29 Oct 2020

HAL is a multi-disciplinary open access archive for the deposit and dissemination of scientific research documents, whether they are published or not. The documents may come from teaching and research institutions in France or abroad, or from public or private research centers.

L'archive ouverte pluridisciplinaire **HAL**, est destinée au dépôt et à la diffusion de documents scientifiques de niveau recherche, publiés ou non, émanant des établissements d'enseignement et de recherche français ou étrangers, des laboratoires publics ou privés.



The relationship between peak warming and cumulative CO₂ emissions, and its use to quantify vulnerabilities in the carbon-climate-human system

Michael R. Raupach, Josep G. Canadell, Philippe Ciais, Pierre Friedlingstein, Peter J. Rayner & Catherine M. Trudinger

To cite this article: Michael R. Raupach, Josep G. Canadell, Philippe Ciais, Pierre Friedlingstein, Peter J. Rayner & Catherine M. Trudinger (2011) The relationship between peak warming and cumulative CO₂ emissions, and its use to quantify vulnerabilities in the carbon-climate-human system, Tellus B: Chemical and Physical Meteorology, 63:2, 145-164, DOI: [10.1111/j.1600-0889.2010.00521.x](https://doi.org/10.1111/j.1600-0889.2010.00521.x)

To link to this article: <https://doi.org/10.1111/j.1600-0889.2010.00521.x>



© 2011 The Author(s). Published by Taylor & Francis.



Published online: 18 Jan 2017.



[Submit your article to this journal](#)



Article views: 244



[View related articles](#)



Citing articles: 46 [View citing articles](#)

The relationship between peak warming and cumulative CO₂ emissions, and its use to quantify vulnerabilities in the carbon–climate–human system

By MICHAEL R. RAUPACH^{1,3*}, JOSEP G. CANADELL^{1,3}, PHILIPPE CIAIS^{2,3},
PIERRE FRIEDLINGSTEIN^{2,3}, PETER J. RAYNER² and CATHERINE M. TRUDINGER⁴,

¹Centre for Atmospheric, Weather and Climate Research, CSIRO Marine and Atmospheric Research, Canberra, ACT, Australia; ²LSCE/IPSL, Laboratoire CEA-CNRS-UVSQ, CEA de Saclay, Gif/Yvette, France; ³ESSP Global Carbon Project, Canberra, Australia; ⁴Centre for Atmospheric, Weather and Climate Research, CSIRO Marine and Atmospheric Research, Aspendale, Victoria, Australia

(Manuscript received 20 December 2009; in final form 22 November 2010)

ABSTRACT

Interactions between the carbon cycle, climate and human societies are subject to several major vulnerabilities, broadly defined as factors contributing to the risk of harm from human-induced climate change. We assess five vulnerabilities: (1) effects of increasing CO₂ on the partition of anthropogenic carbon between atmospheric, land and ocean reservoirs; (2) effects of climate change (quantified by temperature) on CO₂ fluxes; (3) uncertainty in climate sensitivity; (4) non-CO₂ radiative forcing and (5) anthropogenic CO₂ emissions. Our analysis uses a physically based expression for $T_p(Q_p)$, the peak warming T_p associated with a cumulative anthropogenic CO₂ emission Q_p to the time of peak warming. The approximations in this expression are evaluated using a non-linear box model of the carbon–climate system, forced with capped emissions trajectories described by an analytic form satisfying integral and smoothness constraints. The first four vulnerabilities appear as parameters that influence $T_p(Q_p)$, whereas the last appears through the independent variable. In terms of likely implications for $T_p(Q_p)$, the decreasing order of the first four vulnerabilities is: uncertainties in climate sensitivity, effects of non-CO₂ radiative forcing, effects of climate change on CO₂ fluxes and effects of increasing CO₂ on the partition of anthropogenic carbon.

1. Introduction

The magnitude and rate of future human-induced climate change is uncertain because of multiple feedbacks in the earth system, many of which involve interactions between climate and the carbon cycle (Cox et al., 2000; Gruber et al., 2004; Steffen et al., 2004; IPCC, 2001b, 2007b). The implications of positive or reinforcing feedback processes are particularly significant because they lead to positively skewed probability distributions for future climate change (Roe and Baker, 2007; Knutti and Hegerl, 2008), which include non-negligible probabilities for extreme outcomes. Such a risk profile has prompted consideration of earth system ‘vulnerability’, a term which has been defined with different emphases in several disciplines. A definition for human–environment interactions in socio-ecological

systems (Turner et al., 2003) is: ‘vulnerability is the degree to which a system, subsystem, or system component is likely to experience harm due to exposure to a hazard, either a perturbation or stress/stressor’. With an emphasis on climate change, the Intergovernmental Panel on Climate Change (IPCC) defined vulnerability as ‘the degree to which a system is susceptible to, or unable to cope with, adverse effects of climate change, including climate variability and extremes’ (IPCC, 2007a, p883, p783; also IPCC, 2001a, p. 995).

The term ‘vulnerability’ has also been applied to carbon–climate interactions in a narrower sense, to mean the extent to which the build-up of atmospheric CO₂ from anthropogenic emissions may be accelerated by climate change itself through positive carbon–climate feedbacks. Two broad groups of processes are involved, those affecting the natural land and ocean sinks of atmospheric CO₂, and those leading to CO₂ releases from previously immobile stores of carbon on land or in the ocean. The consequences of both groups were investigated by Gruber et al. (2004) using a heuristic, risk-based approach. More

*Corresponding author.

e-mail: michael.raupach@csiro.au

DOI: 10.1111/j.1600-0889.2010.00521.x

quantitatively, carbon–climate model intercomparison experiments (Friedlingstein et al., 2006; Sitch et al., 2008) indicate significant enhancement of climate change by climate-induced effects on land and ocean CO₂ sinks, but with substantial variability between models, especially for the land sink. A number of studies have also addressed specific carbon pools which are vulnerable to disturbance by climate change and/or land use change, such as organic carbon in frozen soils (Zimov et al., 2006; Schuur et al., 2008; Tarnocai et al., 2009) and in tropical peatlands (Hooijer et al., 2009).

In this work we define vulnerabilities broadly, as factors contributing to the risk of harm from human-induced climate change. These factors include both forcings and responses. The definition of ‘harmful’ or ‘dangerous’ climate change is necessarily subjective, involving value judgements about the well being of humankind and the biosphere. One widely used marker is a peak warming of 2 K above pre-industrial temperatures (Schellnhuber et al., 2006). For any nominated marker, the risk of crossing that point can be estimated objectively as a function of the magnitude of anthropogenic forcing on climate and biogeochemical cycles, the biophysical response of the system for a given forcing (the system sensitivity) and uncertainty in both forcing and response.

Our aim is to quantify and rank five vulnerabilities in the carbon–climate–human system, arising from (1) effects of increasing CO₂ on the partition of anthropogenic carbon between atmospheric, land and ocean reservoirs; (2) effects of climate change (quantified by temperature) on CO₂ fluxes, including releases of carbon from previously undisturbed pools; (3) climate sensitivity; (4) changes in non-CO₂ radiative forcing and (5) anthropogenic CO₂ emissions. Of these five, the last two are human forcings and the first three involve biophysical responses. These five vulnerabilities are intercompared by examining their relative effects on peak global temperature (T_p) relative to pre-industrial temperatures, used as a single measure of system response.

The analysis is based on two models for carbon–climate interactions: (1) a new algebraic expression for the peak warming T_p associated with a cumulative total anthropogenic CO₂ emission Q_p [PgC] to the time of peak warming, and (2) a non-linear box model for global CO₂, other greenhouse gases and global temperature, using established formulations. Model 1 is an analytic counterpart of recent model results (Allen et al., 2009; Matthews et al., 2009; Meinshausen et al., 2009; Zickfeld et al., 2009) which found that T_p (induced by CO₂ forcing) is a function of Q_p with a definable uncertainty range. Model 1 yields an approximate algebraic expression for $T_p(Q_p)$ which is useful for two reasons: its structure provides some insight into the ways that vulnerabilities interact, and it is easily amenable to perturbation analysis to quantify and rank uncertainties and their implications for vulnerability. Model 2 is used to further explore the robustness of the relationship between T_p and Q_p , and to evaluate the approximations in model 1.

2. Models

2.1. Algebraic expression for peak warming

Global temperature can be related to radiative forcing by a climate response function, which represents the dynamics of a complex climate model in a low-dimensional representation (Li and Jarvis, 2009; Li et al., 2009). In this representation, a trajectory $R(t)$ of radiative forcing [W m^{-2}] leads to a global temperature perturbation (from a mean pre-industrial state) given by

$$T(t) = \lambda_q \int_0^t R'(\tau) h_T(t - \tau) d\tau, \quad (1)$$

where $h_T(t)$ is the climate response function (the fractional response to a unit step in radiative forcing), t is time from the start of the industrial era, $R'(t) = dR(t)/dt$, and $\lambda_q [\text{K W}^{-1} \text{m}^2]$ is the equilibrium climate sensitivity.¹ By definition, λ_q satisfies

$$T_q = \lambda_q R_q, \quad (2)$$

where T_q is the long-term equilibrium warming in response to a steady radiative forcing R_q .

We are concerned here not with the equilibrium response to steady forcing, but with the transient temperature response $T(t)$ to a forcing trajectory involving a finite cumulative emission of CO₂. This yields a temperature trajectory with a peak at some time t_p , followed by a slow decrease. The peak warming can be characterized by a peak climate sensitivity λ_p , such that

$$T_p = \lambda_p R_p, \quad (3)$$

where $T_p = T(t_p)$ is the peak warming and $R_p = R(t_p)$ is the radiative forcing at the time of peak warming. The peak sensitivity λ_p is akin to, but not the same as, the transient climate sensitivity (T at the time of CO₂ doubling for a 1% y^{-1} CO₂ increase; IPCC, 2001b).

The radiative forcing is approximately the sum of contributions from CO₂, non-CO₂ greenhouse gases (CH₄, N₂O, halocarbons and others) and non-gaseous agents (aerosols, albedo changes, volcanic effects and others). Writing the CO₂ forcing as R_C and lumping all other gaseous and non-gaseous forcings into a total non-CO₂ forcing R_N , we have

$$R(t) = R_C(t) + R_N(t). \quad (4)$$

The CO₂ contribution to radiative forcing is taken to be (IPCC, 2001b, p. 358):

$$R_C(t) = 5.35 \ln \left(\frac{C_A(t)}{C_{A0}} \right), \quad (5)$$

where $C_A(t)$ is the mass of CO₂ in the atmosphere (equal to $2.13[\text{CO}_2](t)$, with C_A in PgC, $[\text{CO}_2]$ the concentration in

¹ Climate sensitivity in units of K per CO₂ doubling is related to the unit used here by $\lambda_q [\text{K}(2 \times \text{CO}_2)^{-1}] = 3.71\lambda_q [\text{K W}^{-1} \text{m}^2]$, where 3.71 W m^{-2} is the assumed radiative forcing for CO₂ doubling (Myhre et al., 1998).

ppm and $2.13 \text{ PgC ppm}^{-1}$ a conversion factor); and $C_{A0} = 2.13[\text{CO}_2]_0$ the pre-industrial mass of atmospheric CO_2 , with $[\text{CO}_2]_0 \approx 280 \text{ ppm}$ the pre-industrial CO_2 concentration. A subscript 0 denotes the pre-industrial equilibrium value of any quantity.

We express the increase in atmospheric CO_2 since pre-industrial times ($C_A - C_{A0}$, in PgC) as the result of three influences: (1) anthropogenic emissions, (2) the effects of increasing CO_2 on the partition of anthropogenic carbon between atmospheric, land and ocean reservoirs and (3) the effects of climate change (quantified by temperature) on the carbon cycle, including both currently active CO_2 fluxes and releases of carbon from previously undisturbed pools. The added atmospheric CO_2 concentration from the first two influences is $A(t)Q(t)$, where $Q(t)$ is the total cumulative anthropogenic CO_2 emission from pre-industrial times to time t , and $A(t)$ is the cumulative airborne fraction (CAF) of CO_2 in the absence of climate (temperature) feedback on the carbon cycle. The cumulative emission $Q(t)$ is the time integral of the total emission flux ($F(t)$) from fossil fuels and other industrial processes including cement production (collectively denoted $F_{\text{Foss}}(t)$) and from net land use change ($F_{\text{LUC}}(t)$). The CAF is the fraction of total cumulative emissions remaining in the atmosphere, $(C_A(t) - C_{A0})/Q(t)$. This accounts for time-integrated effects of land and ocean CO_2 sinks, which have together removed more than half of all cumulative emissions through the industrial era to date. The observed cumulative AF was 0.42 in 2009 (Canadell et al., 2007; Le Quere et al., 2009). This observed quantity is slightly different from the quantity $A(t)$ used in this analysis, which is the CAF without carbon-climate (temperature) feedbacks.

The added CO_2 concentration from the third influence (effect of climate change on the carbon cycle) is expressed as $\gamma T(t)$, where γ [PgC K^{-1}] is the aggregate sensitivity of all land and ocean carbon pools to climate change, including both currently mobile pools (such as soil carbon) and pools which are currently largely immobile but vulnerable to disturbance under climate change (such as carbon in frozen soils). Climate change is parameterized by the single variable $T(t)$, recognizing that release of CO_2 from carbon pools through climate change involves multiple processes which respond not only through warming but also through other physical variables such as precipitation and radiation.

Combining the contributions from all three influences, we have

$$C_A(t) - C_{A0} = A(t)Q(t) - \gamma T(t). \quad (6)$$

Taking t to be the time t_p of peak warming, eqs. (3)–(6) yield

$$T_p = \lambda_p \left[5.35 \ln \left(1 + \frac{A_p Q_p + \gamma T_p}{C_{A0}} \right) + R_{Np} \right], \quad (7)$$

where A_p , Q_p , T_p and R_{Np} are the values of $A(t)$, $Q(t)$, $T(t)$ and $R_N(t)$ at $t = t_p$. We now solve for T_p by using the approximation $\ln(x + h) \approx \ln(x) + h/x$,

taking $x = 1 + A_p Q_p / C_{A0} = C_A(t_p) / C_{A0}$ and $h = \gamma T_p / C_{A0}$. The approximation error is of order h^2 and is less than 1% with reference parameters defined later. The result is

$$T_p \approx \frac{\lambda_p}{1 - g} \left[5.35 \ln \left(1 + \frac{A_p Q_p}{C_{A0}} \right) + R_{Np} \right] \quad (8)$$

$$\text{with } g = \frac{5.35 \lambda_p \gamma}{C_{A0} + A_p Q_p}.$$

The factor $1/(1 - g)$ is the amplification of peak warming by effects of warming on CO_2 fluxes, including both currently active fluxes and releases of carbon from previously undisturbed pools. This form is generically familiar as the amplification arising when a fraction g of the output of a system, the ‘gain’, is added to the system input (Roe and Baker, 2007).

Equation (8) is our algebraic expression for peak warming as a function of forcings (Q_p and R_{Np}) and properties of the carbon-climate system (T_p , A_p and γ), all at the time of peak warming, t_p . Because of the dominant role of CO_2 forcing we often denote this expression as $T_p(Q_p)$, with other dependencies understood. The parameters in eq. (8) correspond to the five sources of vulnerability outlined in the introduction: (1) effects of CO_2 on the partition of anthropogenic carbon are quantified by A_p , (2) effects of climate (temperature) change on the carbon cycle by γ , (3) climate sensitivity by λ_p , (4) non- CO_2 radiative forcing by R_{Np} and (5) CO_2 forcing by Q_p .

Given the definitions of its parameters, eq. (8) is formally exact apart from a linearization with a small error (typically less than 1%). The utility of eq. (8) therefore depends mainly on the robustness with which its parameters can be estimated. In particular, the parameters λ_p and A_p are path-dependent properties of carbon-climate trajectories. The extent and consequences of this path dependency are investigated later.

2.2. Non-linear box model

To investigate the robustness of the relationship $T_p(Q_p)$, and also the properties of parameters in eq. (8), we use a non-linear model for global CO_2 , other greenhouse gases and global temperature. This is a globally averaged or ‘box’ model of the carbon-climate system (Oeschger et al., 1975; Joos et al., 1996 and many others), using well-established formulations. Equations and parameters are given in Appendix A and Tables A1 and A2. The model includes non-linearities in the response of terrestrial carbon assimilation to CO_2 , the buffering of CO_2 in the ocean mixed layer, temperature responses of land-air and ocean-air CO_2 exchanges and the response of radiative forcing to gas concentrations.

Model state variables are carbon masses in the atmosphere, in fast and slow terrestrial biospheric C pools, and in a set of ocean C pools; the atmospheric concentrations of CH_4 , N_2O and halocarbons (represented here only by CFC-11 and CFC-12); and global perturbation temperature components. Forcing

is by specified trajectories for CO₂, CH₄, N₂O and halocarbon emissions, which in turn yield concentrations, radiative forcing and global temperature. Radiative forcing occurs from CO₂, CH₄, N₂O, halocarbons and aerosols. The negative radiative forcing contribution from aerosols is taken to be proportional to total CO₂ emissions (on the assumptions that anthropogenic aerosol inputs are approximately proportional to total CO₂ emissions and removals are rapid), with a proportionality coefficient set to match total radiative forcing in 2005 (Appendix A). Because some non-CO₂ anthropogenic radiative forcings are omitted, the resulting modelled aerosol forcing is likely to underestimate the actual negative aerosol forcing in 2005.

Past emissions trajectories for CO₂ are set from data, and future trajectories are described in the next subsection. For CH₄, N₂O and halocarbons, past emissions are set from data and the requirement that the model match observed concentrations, and future emissions are assumed to follow the IPCC SRES (Special Report on Emissions Scenarios) A1B marker scenario (Nakicenovic et al., 2000). Temperature is related to radiative forcing by eq. (1), using a climate response function of the common form of a sum of decaying exponentials in time (Appendix B) and solved as a set of linear equations (Appendix A). We use a three-term climate response function (Table A2) for the HadCM3 climate model (Li and Jarvis, 2009) with its associated climate sensitivity, $\lambda_q = 1.235 \text{ K W}^{-1} \text{ m}^2$.

Model parameters were selected for consistency with past data, accounting for prior constraints (see Table A2 for values). The temperature part of the model is parameterized entirely by the three-term HadCM3 climate response function and its equilibrium climate sensitivity.

The value $\lambda_q = 1.235 \text{ K W}^{-1} \text{ m}^2$ for the equilibrium climate sensitivity from the HadCM3 model is significantly higher than many recent estimates, which are typically $3(2 \text{ to } 4.5) \text{ K}(2 \times \text{CO}_2)^{-1}$ or $0.81(0.54 \text{ to } 1.21) \text{ K W}^{-1} \text{ m}^2$ (IPCC, 2007b, p. 66; also see Meinshausen, 2006; Knutti and Hegerl, 2008). The wide and positively skewed uncertainty in the equilibrium climate sensitivity reflects both uncertainty and asymmetry in the effects of climate feedbacks, for instance through water vapour, clouds and aerosols (Roe and Baker, 2007; Knutti and Hegerl, 2008). The value $\lambda_q = 1.235 \text{ K W}^{-1} \text{ m}^2$ is high because the longest time scale in the three-term HadCM3 climate response function (Li and Jarvis, 2009) is nearly 1500 years, long enough to include slow feedbacks such as ocean and cryosphere responses which are often not included in determinations of climate sensitivity but which contribute to the full ‘earth system’ sensitivity (Hansen et al., 2008). There is an association between the long-term equilibrium sensitivity and the long time scales of a climate or earth system model, although transient responses are better constrained by observed temperature trends (Frame et al., 2006). The uncertainty in equilibrium climate or earth system sensitivity arises mainly from uncertainty about slow feedbacks and responses.

2.3. CO₂ emissions trajectories

The CO₂ emission flux [PgC y^{-1}] from fossil fuels and other industrial processes is specified with an emissions trajectory defined by

$$F_{\text{Foss}}(t) = \begin{cases} \text{observations} & (t \leq t_1), \\ F_m \exp(r(t - t_m)) & (t_1 < t \leq t_m), \\ f(t) & (t > t_m), \end{cases}$$

$$f(t) = F_m [1 + (r + m)(t - t_m)] \exp(-m(t - t_m)). \quad (9)$$

Here t_1 is the time to which observations are available, t_m is the time in the future at which mitigation begins, F_m is the emission at time t_m , r [y^{-1}] is the proportional growth rate of $F_{\text{Foss}}(t)$ before mitigation, and m [y^{-1}] is an applied mitigation rate. This ‘smooth capped’ emissions trajectory merges an exponential growth phase with growth rate r , applicable for $t \leq t_m$, with a mitigation phase starting at $t = t_m$ in which emissions follow the trajectory $f(t)$, initially increasing at growth rate r and ultimately decreasing exponentially at the mitigation rate m . Emissions reach their maximum after $t = t_m$ because initial growth must be overcome.

The all-time cumulative emission [PgC] is the finite quantity

$$Q_{\text{Foss}}(\infty) = \int_{t_0}^{\infty} F_{\text{Foss}}(t) dt$$

$$= Q_{\text{Foss}}(t_1) + \frac{F_m}{r} [1 - \exp(r(t - t_m))] + \frac{F_m(2m + r)}{m^2}, \quad (10)$$

where the three terms on the right-hand side are respectively the contributions to the integral from the past ($t \leq t_1$), future pre-mitigation ($t_1 < t \leq t_m$) and mitigation ($t > t_m$) phases of eq. (9). The initial time (t_0) is taken as 1751.

Using data from sources given in Appendix C, cumulative fossil-fuel emissions from 1751 to the end of 2008 (denoted as $t_1 = 2008.99$) were $Q_{\text{Foss}}(t_1) = 346 \text{ PgC}$, and F_{Foss} in 2008 was 8.67 PgC y^{-1} . The growth rate of F_{Foss} for the decade 2000.00–2009.99 was $r = 0.03 \text{ y}^{-1}$, a value which includes an estimate of the effect of the recent global financial crisis (Le Quere et al., 2009; Raupach and Canadell, 2010).

In this work, net CO₂ emissions from land use change ($F_{\text{LUC}}(t)$) are specified simply by past emissions to time $t_1 = 2008.99$ (Houghton, 2003; Le Quere et al., 2009) and a linear decrease in the future to zero at $t = 2100$. Cumulative net CO₂ emissions from land use change were 160 PgC from 1850 to the end of 2008. To estimate cumulative land use change emissions before 1850, we assume a linear increase from zero in 1751 to 0.5 PgC y^{-1} for 1850, the earliest available estimate (Houghton, 2003). This implies an additional 25 PgC of cumulative emission before 1850. The resulting cumulative land use change emission from 1751 onwards is $Q_{\text{LUC}}(t) = 185 \text{ PgC}$ to $t_1 = 2008.99$.

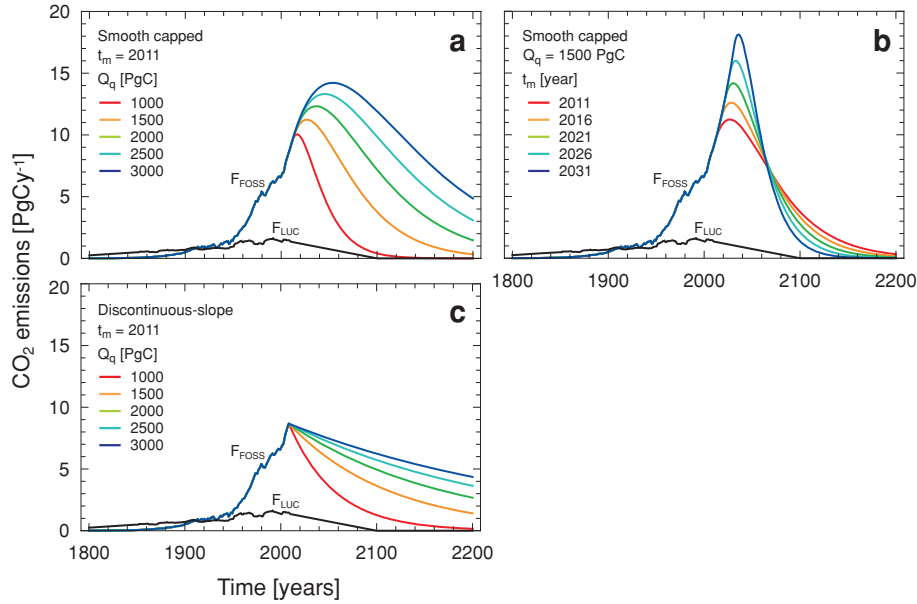


Fig. 1. Capped trajectories for CO₂ emissions from fossil fuels and other industrial sources (F_{FOSS} , colours), and emissions from land use change (F_{LUC} , black). Total ($F_{\text{FOSS}} + F_{\text{LUC}}$) emissions integrate over all time to indicated quotas Q_q from 1000 to 3000 PgC. (a) Smooth capped trajectories for F_{FOSS} from eq. (9), with Q_q varying from 1000 to 3000 PgC and mitigation start time $t_m = 2011$. (b) As for (a), with t_m varying from 2011 to 2031 and $Q_q = 1500$ PgC. (c) Discontinuous-slope capped trajectories from eq. (12), with Q_q varying from 1000 to 3000 PgC and $t_m = 2011$. In all panels, growth rate in F_{FOSS} at time t_m is $r = 0.03 \text{ y}^{-1}$.

Figures 1a and b show capped trajectories for CO₂ emissions from fossil fuels ($F_{\text{FOSS}}(t)$) from eq. (9), together with net land use change ($F_{\text{LUC}}(t)$) specified as above. In these trajectories, there is a specified cap

$$Q_q = Q_{\text{FOSS}}(\infty) + Q_{\text{LUC}}(\infty)$$

for the all-time total cumulative CO₂ emission from both fossil fuels and land use change, from 1751 to the far future. In Fig. 1a, Q_q varies among curves with a fixed mitigation start time t_m in eq. (9), whereas in Fig. 1b, t_m varies among curves with fixed Q_q . As Q_q increases with fixed t_m , peak emissions occur progressively later and the subsequent decay rate decreases (Fig. 1a). As the start of mitigation (t_m) is delayed with a given cap Q_q , peak emissions occur later but the subsequent decay rate increases sharply (Fig. 1b).

We can write Q_q as a sum of four components:

$$Q_q = \text{past } Q_{\text{FOSS}} + \text{future } Q_{\text{FOSS}} + \text{past } Q_{\text{LUC}} + \text{future } Q_{\text{LUC}}. \quad (11)$$

From the above data, past $Q_{\text{FOSS}} = 346 (\pm 50)$ PgC and past $Q_{\text{LUC}} = 185 (\pm 70)$ PgC, taking the past-future divide as $t_1 = 2008.99$ and showing heuristic uncertainty estimates in brackets. Under the above assumed trajectory for future $F_{\text{LUC}}(t)$, we have future $Q_{\text{LUC}} = 70 (\pm 50)$ PgC. (Although future land use change emissions are subject to human management like fossil fuel emissions, future Q_{LUC} is likely to be much smaller than future Q_{FOSS} and is prescribed here for simplicity). The sum of

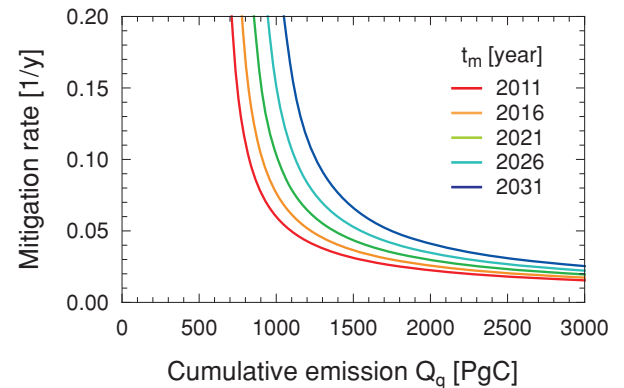


Fig. 2. Mitigation rate m as a function of all-time cumulative emission Q_q , for smooth capped emissions trajectories (eq. 9) with $r = 0.03 \text{ y}^{-1}$ and with mitigation start time t_m varying from 2011 to 2031. Colours correspond with Fig. 1b, which shows trajectories for $F_{\text{FOSS}}(t)$ with the same values of t_m at $Q_q = 1500$ PgC. Components of Q_q other than F_{FOSS} are specified by eq. (11) and following text.

past Q_{FOSS} , past Q_{LUC} and future Q_{LUC} yields a total commitment apart from future Q_{FOSS} of $600 (\pm 100)$ PgC to nearest 10 PgC, with root-mean-square summation of uncertainties. The future quota for Q_{FOSS} is less than any nominated value of Q_q by this amount.

Figure 2 shows the mitigation rate m required to achieve a given Q_q , for five mitigation start times t_m between 2011 and

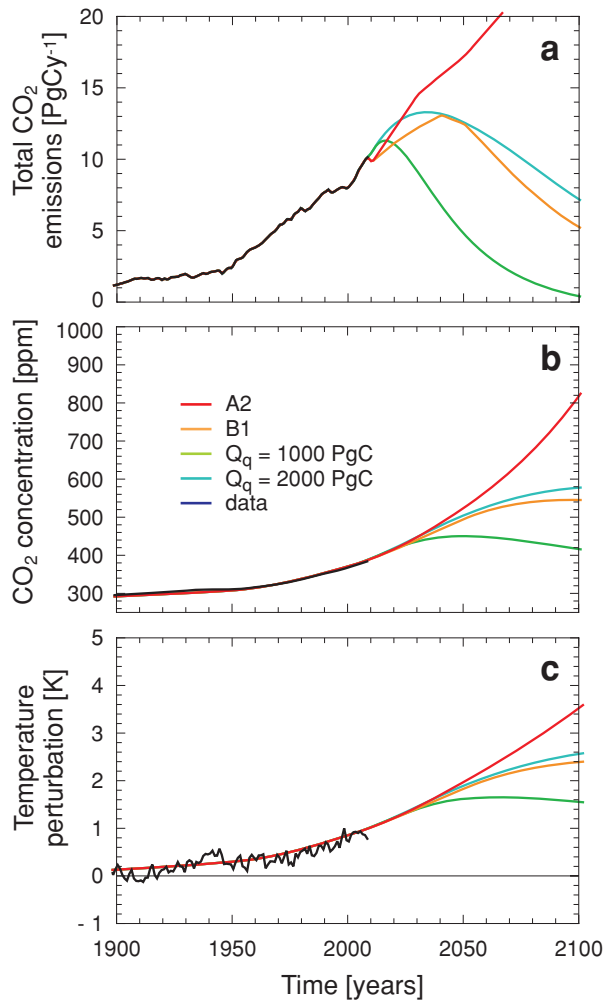


Fig. 3. Trajectories of CO₂ emissions, CO₂ concentrations and temperature from non-linear box model, with four emissions trajectories for F_{Foss} : IPCC SRES marker scenarios A2 and B1 (Nakicenovic et al., 2000), and smooth capped trajectories (eq. 9 and Fig. 1) with all-time cumulative emissions $Q_q = 1000$ and 2000 PgC and mitigation start time $t_m = 2011$. See Appendix C for data sources. Radiative forcing is from CO₂ only.

2031. (Emissions up to t_m are assumed to continue growing exponentially; see eq. 9). As Q_q decreases, the required mitigation rate m increases sharply, and higher rates m are needed as t_m becomes later. This figure quantifies the increase in the mitigation challenge (specified by m) with delay (specified by t_m).

Figure 1c shows an alternative ‘discontinuous-slope’ model for capped future emissions,

$$F_{\text{Foss}}(t) = \begin{cases} \text{observations} & (t \leq t_1), \\ F_m \exp(r(t - t_m)) & (t_1 < t \leq t_m), \\ F_m \exp(-m(t - t_m)) & (t > t_m). \end{cases} \quad (12)$$

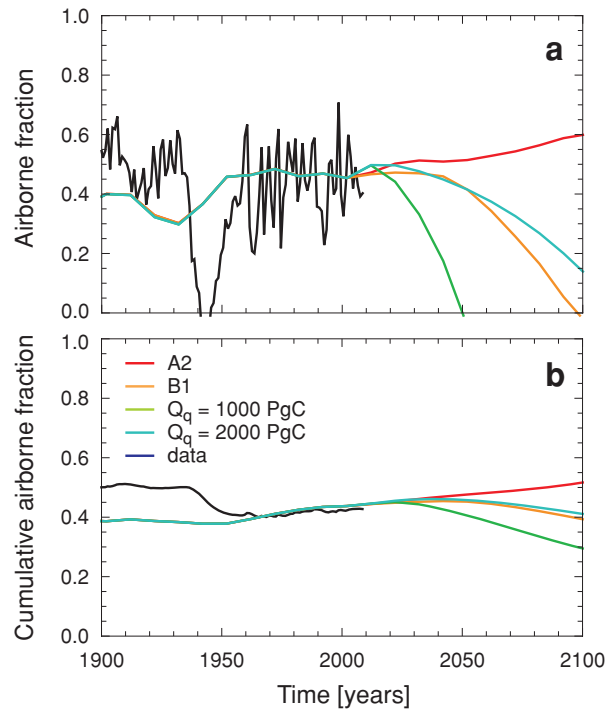


Fig. 4. Trajectories of airborne fraction and cumulative airborne fraction from non-linear box model, for the same conditions as in Fig. 3. See Appendix C for data sources.

These trajectories have a slope discontinuity at the mitigation start time t_m , and are therefore ignore the effects of technological inertia in propagating patterns of CO₂ emissions and carbon intensities over decades (Raupach et al., 2007). They provide an extreme test of the path dependence of parameters in eq. (8).

3. Results

3.1. Non-linear box model with radiative forcing from CO₂ only

Figure 3 shows trajectories of total CO₂ emissions ($F_{\text{Foss}} + F_{\text{LUC}}$), CO₂ concentrations and temperature from the non-linear box model, with forcing from CO₂ only, under four CO₂ emissions scenarios: IPCC SRES A2 and B1 marker scenarios (Nakicenovic et al., 2000), and smooth capped trajectories (eq. 9, Fig. 1a) with $Q_q = 1000$ and 2000 PgC. Observed data (shown as black lines) are from sources specified in Appendix C.

With forcing from the IPCC SRES A2 and B1 marker scenarios, the temperature trajectories are well within the range from full climate models in the IPCC Fourth Assessment (IPCC, 2007b), although slightly lower than best-estimate IPCC projections (consistent with the omission of non-CO₂ forcings in Fig. 3). Temperature trajectories with capped emissions decline after a peak temperature is reached, but only slowly (Lowe et al., 2009; Solomon et al., 2009) (also see Figs 5–8).

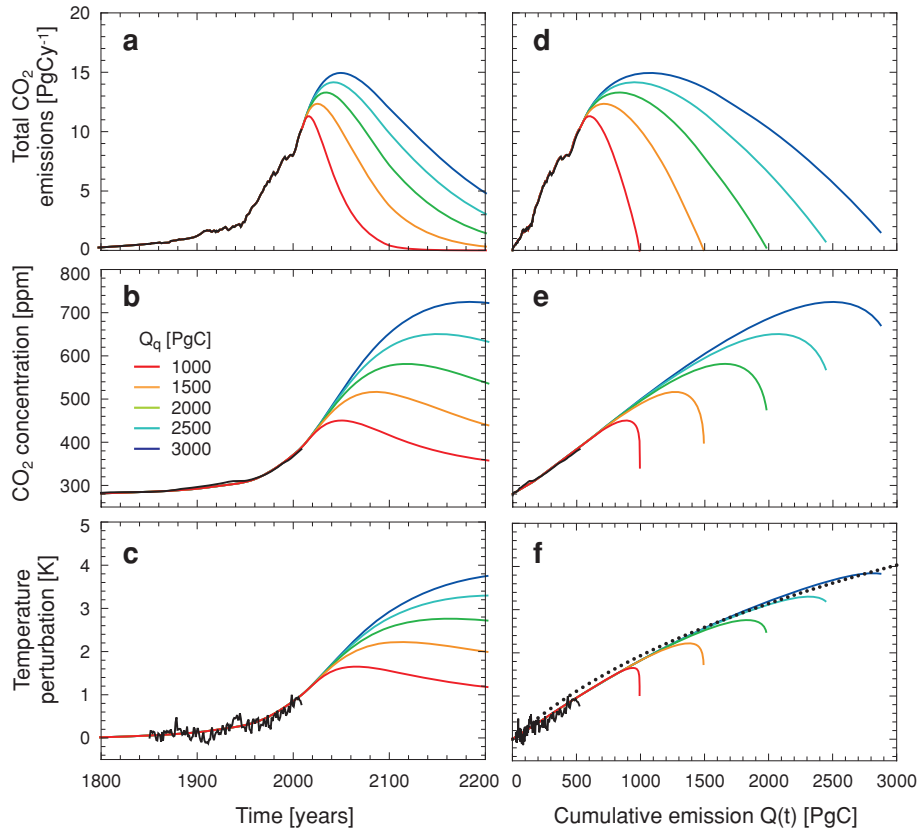


Fig. 5. Total CO₂ emissions ($F_{\text{Foss}} + F_{\text{LUC}}$), CO₂ concentrations and temperatures from the nonlinear box model (coloured curves), for smooth capped CO₂ emissions trajectories (eq. (9)) with all-time cumulative emission Q_q from 1000 to 3000 PgC and mitigation start time fixed at $t_m = 2011$, as in Fig. 1a. Black curves are observations (see Appendix C for data sources). Radiative forcing is from CO₂ only. Quantities are plotted against time in left panels (a, b, c) and cumulative CO₂ emissions $Q(t)$ in right panels (d, e, f). Dotted curve in Fig. 5f is from the algebraic expression for $T_p(Q_p)$, eq. 8, with reference parameters.

Figure 4 shows the modelled CO₂ airborne fraction (AF, over annual increments) and cumulative airborne fraction (CAF, defined above), for the same scenarios and conditions as Fig. 3. Agreement with past data (derived from sources in Appendix C) is broadly good, although with departures before 1950 when anthropogenic forcing of the carbon cycle was relatively much weaker than in recent decades. The cumulatively smoothed character of the CAF means that there is much less interannual variability in observations of the CAF than the AF, and also that there is less variation future projections of the CAF than the AF. By 2100, the CAF is projected to be about 0.5 (A2 emissions scenario) and 0.4 (B1), respectively, whereas the AF projections are 0.6 (A2) and 0 (B1).

Figure 5 shows total CO₂ emissions ($F_{\text{Foss}} + F_{\text{LUC}}$), CO₂ concentration and temperature from the non-linear box model, for smooth capped CO₂ emissions trajectories (eq. 9) with all-time quotas Q_q from 1000 to 3000 PgC, and radiative forcing from CO₂ only. In the left panels (Figs 5a–c) the trajectories are plotted conventionally against time, while in the corresponding right panels (Figs 5d–f) they are plotted against the cumulative emission to time t , $Q(t)$. Plots using this ‘cumulative emission

clock’ take the form of curves such as $[\text{CO}_2](Q)$ and $T(Q)$, in which time varies parametrically along each curve.

Three results are evident in Fig. 5. First, there are successive delays between the times of peak emissions, peak CO₂ concentration and peak temperature, both in the plots against t (Figs 5a–c) and against $Q(t)$ (Figs 5d–f). The delays become greater at higher quotas Q_q and therefore higher peak warmings.

Secondly, the temperature trajectories $T(Q)$ in Fig. 5f (using the cumulative emission clock) show an approximate collapse to a common curve up to near the point of maximum temperature, which occurs at time t_p or at cumulative emission $Q_p = Q(t_p)$. Temperatures fall below this curve at later times. The common curve is approximately represented by the dotted line in Fig. 5f, which provides a point of reference (it represents the algebraic expression for peak warming, eq. 8, as described later).

Thirdly, by the time t_p of peak temperature, most of the total cumulative emission quota has already been released. The maximum temperature $[T_p = T(t_p)]$ occurs at a cumulative emission Q_p which is less than the all-time quota Q_q by only about 2% at $Q_q = 1000$ PgC and 10% at $Q_q = 3000$ PgC.

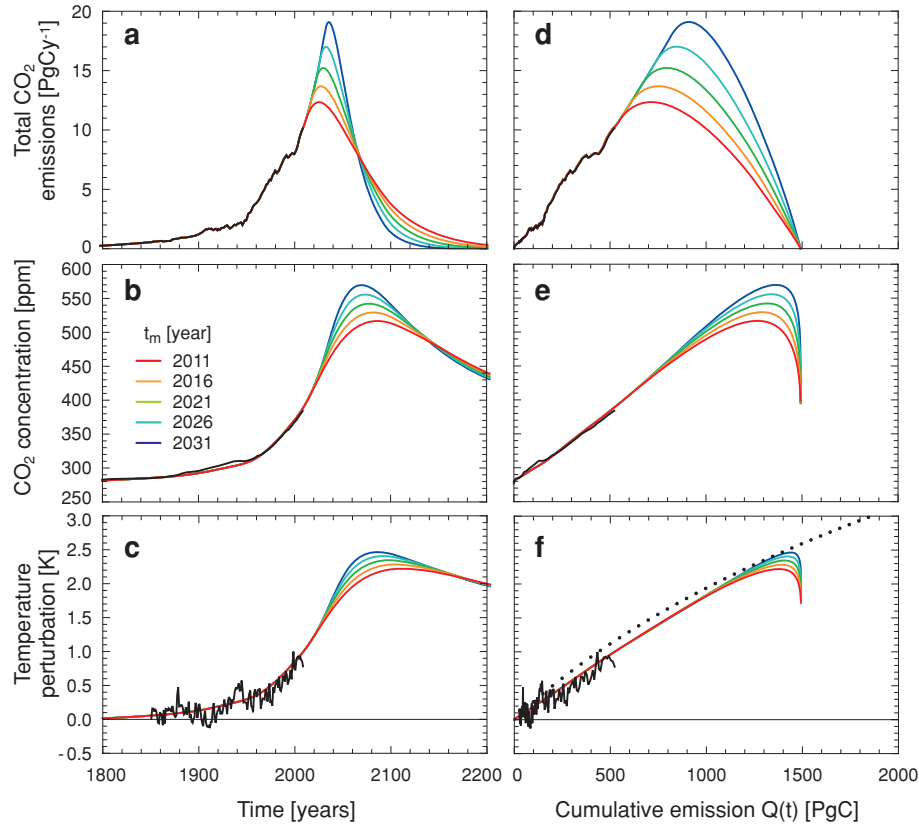


Fig. 6. Total CO₂ emissions ($F_{\text{Foss}} + F_{\text{LUC}}$), CO₂ concentrations and temperatures from the nonlinear box model (coloured curves), for smooth capped CO₂ emissions trajectories (eq. 9) with mitigation start time t_m varying from 2011 to 2031 and all-time cumulative emission fixed at $Q_q = 1500$ PgC, as in Fig. 1b. Other details are as for Fig. 5.

It is important to test the extent to which the results in Fig. 5 (and others discussed later) depend upon properties of the assumed family of CO₂ emissions trajectories (eq. 9). One such property is that the time of the peak in emissions occurs progressively later with larger all-time cumulative emissions Q_q . Although this behaviour is likely for emissions scenarios which peak and decline to yield finite all-time integrals, it is not inevitable. Therefore, the analysis of Fig. 5 is repeated in Figs 6 and 7 with two alternative families of emissions trajectories which decouple the relationship between Q_q and the time of peak emissions. Figure 6 uses a set of emissions trajectories with the same Q_q but different times for peak emissions, whereas Fig. 7 uses emissions trajectories with the same time of peak emissions but varying Q_q .

The emissions trajectories in Fig. 6 are obtained from the smooth capped trajectory family, eq. (9), by varying the mitigation start time t_m from 2011 to 2031 with fixed Q_q (1500 PgC) as in Fig. 1b. Peak emissions occur within a few years of t_m for all these trajectories, but the rate at which emissions fall after the peak increases rapidly with delay in starting mitigation. This occurs because increased delay (later t_m) increases the cumulative emissions expended before t_m , so a faster decline after the peak

in emissions is necessary to meet the constraint of a fixed Q_q . For this family of emissions trajectories, the times of peak CO₂ concentration and peak temperature occur progressively earlier for progressively later times of peak emissions (Figs 6a–c). This initially counterintuitive behaviour, which contrasts with Figs 5a–c, occurs because of the progressively sharper fall in emissions with delay in t_m . However, when trajectories are plotted against the cumulative emission clock (Figs 6d–f), the expected order of peak occurrences is recovered: delay in t_m moves the peaks in emissions, CO₂ concentration and temperature to larger $Q(t)$.

The other two main results from Fig. 5 [the collapse of $T(Q)$ to a common curve up to near $Q_p = Q(t_p)$, and the fact that Q_p is nearly all of the all-time quota Q_q] are also evident in Fig. 6.

In Fig. 7, emissions trajectories with the same time of peak emissions but varying Q_q are obtained from the discontinuous-slope emissions trajectory (eq. 12) with mitigation start time $t_m = 2011$ as in Fig. 1c, thus forcing the peak emission to occur at this time for all Q_q . In this case, all three main results from Fig. 5 are also observed, but the common curve to which $T(Q)$ collapses (for Q nearly up to Q_p) is slightly lower than the

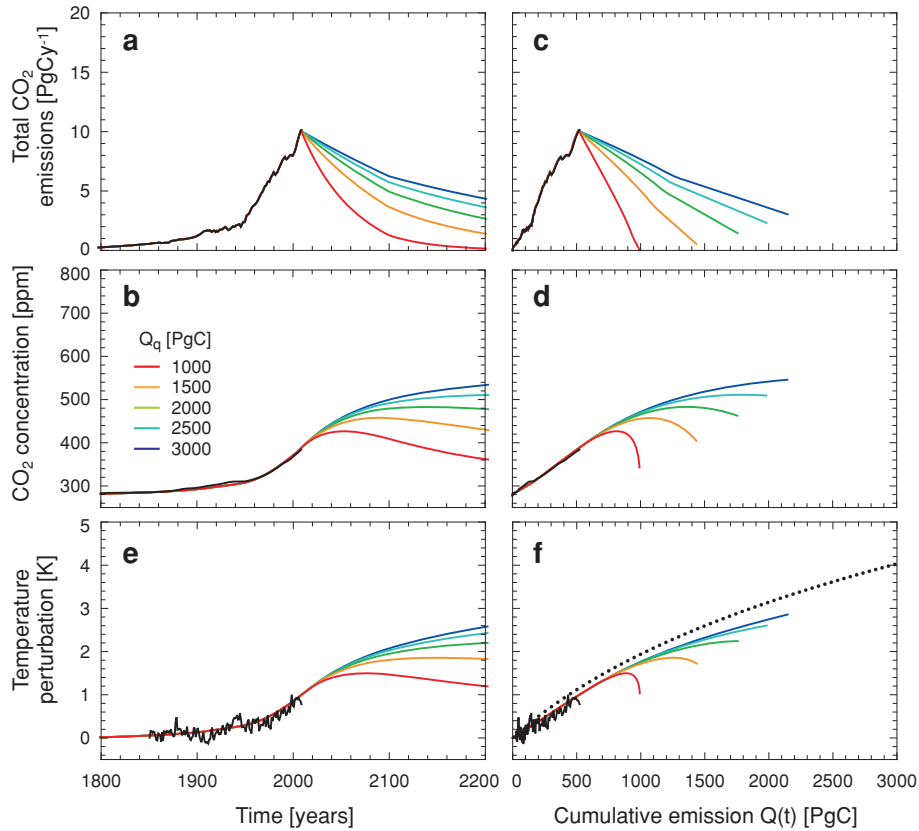


Fig. 7. Total CO₂ emissions ($F_{\text{Foss}} + F_{\text{LUC}}$), CO₂ concentrations and temperatures from the nonlinear box model, for discontinuous-slope capped CO₂ emissions trajectories (eq. (12)) with all-time cumulative emission Q_q from 1000 to 3000 PgC and mitigation start time fixed at $t_m = 2011$, as in Fig. 1c. Other details are as for Fig. 5.

curve in Figs 5 and 6. Therefore, this common curve is weakly dependent on the family of emissions trajectories.

3.2. Non-linear box model with multigas radiative forcing

Here we examine the response of temperature trajectories to radiative forcing from multiple agents, to assess the effect of non-CO₂ radiative forcing on the collapse of $T(Q)$ to a common curve. For these calculations, future anthropogenic emissions of the non-CO₂ greenhouse gases considered here (CH₄, N₂O and halocarbons, represented only by CFCs) were prescribed using a simple illustrative scenario given in Appendix A. The (negative) radiative forcing from aerosols was assumed to be proportional to total CO₂ emissions (Section 2 and Appendix A).

The multigas radiative forcings following from these assumptions are shown in Fig. 8a. The total radiative forcing (blue curve) is approximately equal to the CO₂-only forcing (red curve) in 2000, consistent with the approximate cancellation in the recent past of radiative forcing from non-CO₂ gases and non-gaseous agents. The estimated total radiative forcing in 2005 was +1.6

(0.6–2.4) W m⁻² (IPCC, 2007b), including contributions of +1.6 W m⁻² from CO₂, +1.4 W m⁻² from non-CO₂ gases (CH₄, N₂O and others), and -1.5 W m⁻² from non-gaseous agents, mainly direct and indirect aerosol forcing of -1.2(-2.7 to -0.4) W m⁻², which contributed the largest uncertainty. In future, however, the positive forcing from non-CO₂ gases is likely to increase and negative forcing from aerosols is likely to decrease, as suggested by detailed models of non-CO₂ radiative forcings (Strassmann et al., 2009). This means that total radiative forcing in the long-term (century scale) future is likely to significantly exceed the CO₂-only forcing. Figure 8a reflects this expectation, and also suggests that there will be a short-term (decadal-scale) increase in negative radiative forcing from aerosols as CO₂ emissions increase, causing total radiative forcing to fall below the CO₂-only forcing for a few decades.

The temperature trajectories resulting from these radiative forcings are shown in Figs 8b and c, plotted respectively against t and the cumulative emission clock $Q(t)$. In the immediate future, temperatures fall below the common curve for CO₂-only forcing, but temperatures subsequently rise to peaks above this

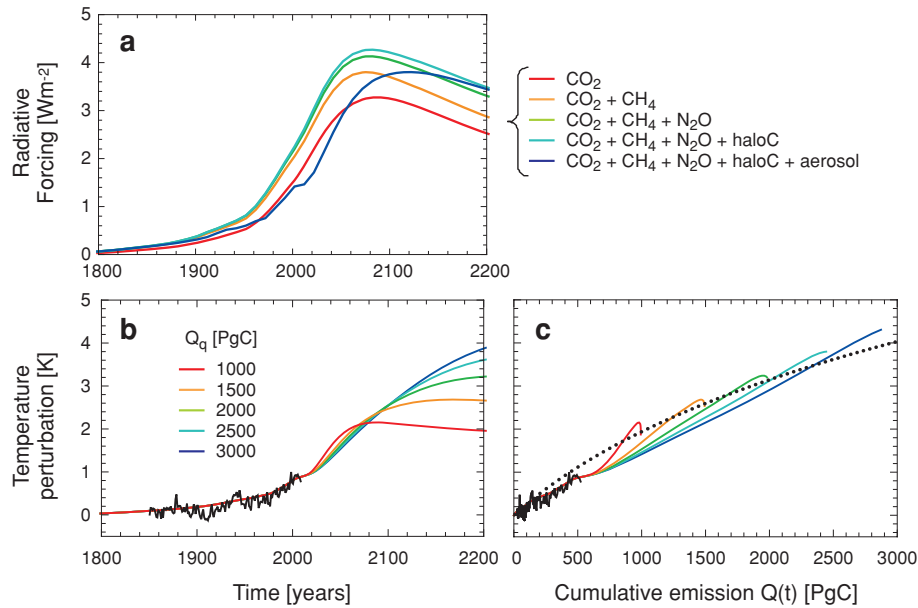


Fig. 8. (a) Cumulative contributions to multi-gas radiative forcing from CO₂, CH₄, N₂O, halocarbons and aerosols. Radiative forcing for CO₂ assumes smooth capped CO₂ emissions trajectory (eq. 9) with $Q_q = 1500$ PgC and $t_m = 2011$. Radiative forcing for CH₄, N₂O and halocarbons (represented by CFC-11 and CFC-12) uses a simple illustrative emissions scenario (Appendix A). Radiative forcing for aerosols is assumed proportional to CO₂ emissions (Appendix A). (b) Temperature trajectories from nonlinear box model plotted against time t , with multigas radiative forcing assuming smooth capped CO₂ emissions trajectories (eq. (9)) with Q_q from 1000 to 3000 PgC and $t_m = 2011$, and multigas forcing as in (a). (c) Temperature trajectories as in (b) but plotted against cumulative CO₂ emissions clock $Q(t)$. Other details are as for Fig. 5.

curve because of the extra radiative forcing from non-CO₂ gases and the progressive decrease in negative forcing from aerosols.

3.3. Path dependence

We now assess the path dependence of the parameters λ_p and A_p in eq. (8). It is shown in Appendix B that the peak climate sensitivity λ_p depends on the trajectory of radiative forcing, unlike the equilibrium climate sensitivity λ_q which (under a linear climate model) is independent of the path to equilibrium. System inertia suggests that λ_p is less than λ_q , because the system at time t_p has realised only a fraction of its ultimate equilibrium response. Therefore, it is appropriate to investigate the ratio λ_p/λ_q as a measure of the path dependence of λ_p .

By contrast, the CAF $A(t)$ is approximately steady in conditions where emissions are increasing approximately exponentially, as has occurred over the past century or more. As the system approaches a long-term equilibrium in which emissions are zero, $A(t)$ is expected to decline (Fig. 4). Therefore, a suitable measure of path dependence in A_p is the ratio A_p/A_m , where A_m is the CAF at the time t_m when mitigation begins.

Figure 9 shows the calculated dependence (from the nonlinear box model) of the ratios λ_p/λ_q and A_p/A_m on the all-time cumulative emission Q_q , for three emissions scenarios: first (coloured lines) for CO₂ forcing with smooth capped CO₂ emissions trajectories (eq. 9 and Fig. 5) in which the mitigation start time

t_m varies from 2011 to 2031 as in Fig. 6; second (solid black curve) for CO₂ forcing with discontinuous-slope capped CO₂ emissions trajectories, taking $t_m = 2011$ as in Fig. 7; and third (grey curve) for multigas radiative forcing as in Fig. 8. These three sets of scenarios test the response of λ_p/λ_q and A_p/A_m to variations of future CO₂ emissions trajectories with several alternative relationships between the all-time cumulative quota Q_q and the time of peak emissions (as in Figs 5–7), and also to the inclusion of non-CO₂ forcings (as in Fig. 8).

Figure 9a shows that λ_p/λ_q increases with Q_q , consistent with the above expectation. There is very little dependence on the time of peak emissions when this is varied independently of Q_q (comparing the coloured lines in Fig. 9a), and a response of only a few percent to the inclusion of non-CO₂ forcings as in Fig. 8 (comparing the red and grey lines). There is a slightly larger difference between the smooth capped and discontinuous-slope emissions trajectories (comparing the red and solid black lines).

In summary, the path dependence in λ_p/λ_q is not large, and $\lambda_p/\lambda_q \approx 0.6$ to within 10% for the scenarios investigated. Combining this value with $\lambda_q = 1.235 \text{ K W}^{-1} \text{ m}^2$ for the three-term HadCM3 climate response function (Li and Jarvis, 2009), we find a reference value for λ_p of $0.74 \text{ K W}^{-1} \text{ m}^2$. We have also confirmed that similar values of λ_p are obtained with other climate response functions (Den Elzen et al., 1999; Trudinger and Enting, 2005) with shorter climate response times, arising from

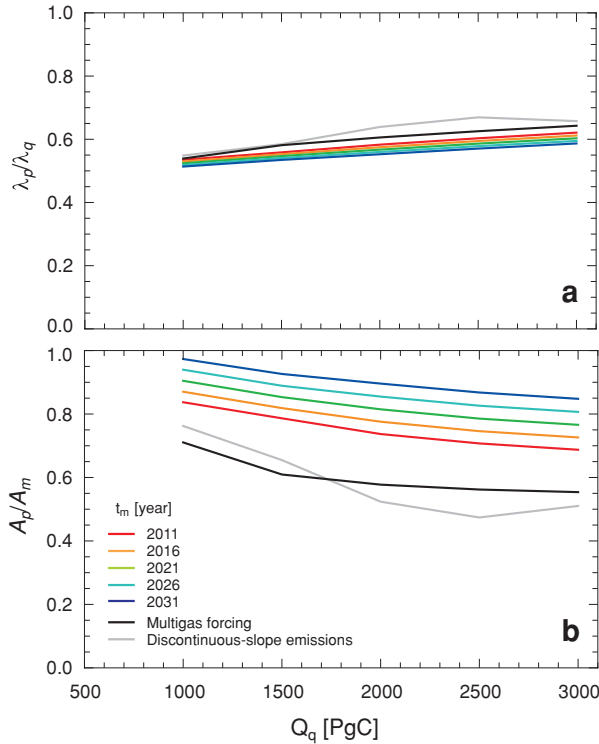


Fig. 9. (a) Ratio λ_p/λ_q and (b) ratio A_p/A_m , plotted against all-time cumulative CO₂ emissions Q_q . Coloured lines are for CO₂ forcing only as in Figs 5 and 6, using smooth capped CO₂ emissions trajectories (eq. 9) and mitigation start time t_m varying from 2011 to 2031. Solid black curve is for CO₂ forcing only as in Fig. 7, using discontinuous-slope capped CO₂ emissions trajectories with $t_m = 2011$. Grey curve is for multigas radiative forcing as in Fig. 8.

example from lower ocean mixing. These climate response functions have lower equilibrium sensitivities λ_q . However, they also yield larger λ_p/λ_q values than those in Fig. 9a (results not shown), leading to similar values for λ_p . The peak sensitivity λ_p is a measure of transient rather than equilibrium climate response, and is therefore relatively consistent across climate models with similar transient responses even if their long-term equilibrium responses are different. Climate models tend to have similar transient responses because they are constrained by observed twentieth century warming (Frame et al., 2006).

Figure 9b shows that A_p/A_m decreases with increasing Q_q in most cases. There is a wider variation in A_p/A_m than in λ_p/λ_q , particularly as the time of peak emissions is delayed by delaying the mitigation start time t_m (comparing the coloured curves in Fig. 9b). This occurs because $A(t)$ increases with time for strongly increasing emissions, and decreases with time when emissions decrease significantly (Fig. 4b).

For cumulatively capped CO₂ emissions scenarios with an immediate start to mitigation ($t_m = 2011$), Fig. 9b shows that A_p/A_m is within 15% of 0.7. Taking the present (2005–2009)

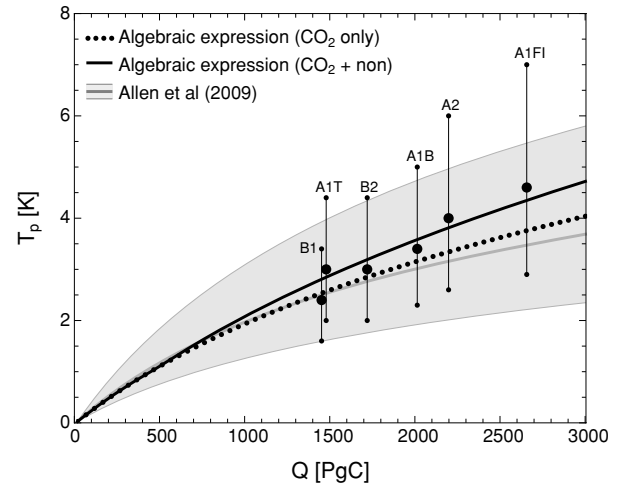


Fig. 10. Peak temperature relative to pre-industrial times, T_p , as a function of all-time cumulative emission Q_q . Dotted line: algebraic expression, eq. (8), with reference parameters, including no non-CO₂ radiative forcing. Solid black line: Eq. (8) with non-CO₂ forcing from eq. (13), taking $s_N = 0.00033 \text{ W m}^{-2} \text{ PgC}^{-1}$. Grey lines: approximations to results of Allen et al. (2009), representing median and 5% and 95% confidence intervals in the distribution of T_p with given Q_p . The median curve is $T_p(Q_p) = 2.076 \ln(1 + Q_p/621.9)$, a fit to the white crosses in Fig. 2 of Allen et al. (2009), and the 5% and 95% curves are multiples of this curve from their Fig. 3. Black points: IPCC scenario results for $(Q(2100), T(2100))$.

CAF to be $A_m = 0.42$ (Canadell et al., 2007; Le Quere et al., 2009; Fig. 4b), we obtain $A_p = 0.29$ as a reference value.

The trends in λ_p/λ_q and A_p/A_m with Q_q in Figs 9a and b are not only opposite but are approximately complementary. This may be partly attributable to the fact that both curves are strongly dependent on the penetration rate for a tracer into the ocean. This nearly complementary behaviour means that compensating errors are introduced into the expression for $T_p(Q_p)$, eq. (8), by variation of λ_p/λ_q and A_p/A_m with cumulative emissions expressed as either Q_q or Q_p (recalling that Q_p is typically 90% or more of Q_q). The effects of variation of Q_p on the parameters λ_p and A_p in eq. (8) are therefore relatively small.

3.4. Algebraic expression for peak warming

The expression for $T_p(Q_p)$ in eq. (8) depends on four parameters, of which three (λ_p , A_p , γ) are properties of the carbon–climate system and one (R_{Np}) is an additional forcing variable together with Q_p . Reference values for these parameters are assigned as follows.

For the peak climate sensitivity (λ_p) and cumulative AF at time of peak temperature (A_p), we use the reference values $\lambda_p = 0.74 \text{ K W}^{-1} \text{ m}^2$ and $A_p = 0.29$ (see previous subsection). This is motivated by the nearly complementary behaviour of λ_p/λ_q and A_p/A_m with variation of Q_p .

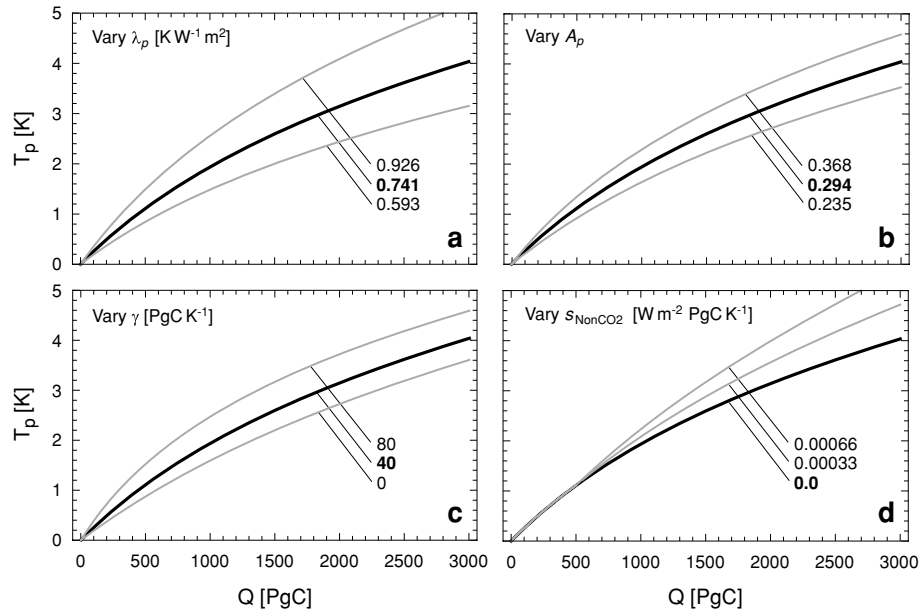


Fig. 11. $T_p(Q_p)$ from eq. (8), showing effects of variation of λ_p , A_p , γ and s_N through specified ranges around reference values (black lines and bold values).

The sensitivity of carbon pools to climate change (γ) is chosen so that g , the gain in eq. (8), is typical of the gain due to climate responses of both land and ocean carbon pools found from models. The C4MIP study (Friedlingstein et al., 2006) compared 11 models forced with an A2 emissions scenario, finding $g \approx 0.15$ (range 0.04–0.31). A later study (Sitch et al., 2008), with five models forced with several emissions scenarios, found similarly scattered but higher values of g (range 0.14–0.43). We choose γ conservatively to give a gain $g = 0.15$ when $Q_p = 1500$ PgC and with other parameters as above, implying a reference value $\gamma = 40$ PgC K⁻¹.

We take a reference value of the non-CO₂ radiative forcing at the time of peak temperature, R_{Np} , to be zero. This is consistent with the approximate cancellation in the recent past of forcing from non-CO₂ gases and non-gaseous agents. However, as noted in Section 3.2 and Fig. 8a, such cancellation is not likely to continue. Radiative forcing from aerosols is likely to become less negative (Ramanathan and Feng, 2008) and the positive forcing from non-CO₂ gases is likely to increase (Strassmann et al., 2009), driven partly by increasing CH₄ and N₂O emissions as agricultural production expands with world population and affluence. Both effects will increase R_{Np} , with consequences to be assessed later.

Figure 10 shows the relationship $T_p(Q_p)$ from eq. (8), with parameters set to the above reference values (dotted curve). This is compared with two other sources of information. First, Allen et al. (2009) and Meinshausen et al. (2009) presented results from multiple carbon–climate models on the peak warming T_p in response to given cumulative emissions. The grey curves in Fig. 10 show the median estimate of T_p and the values at 5%

and 95% confidence intervals, from Allen et al. (2009). There is good agreement between the curve for $T_p(Q_p)$ from eq. (8) with reference parameters (including $R_{Np} = 0$), and the median curve from Allen et al. (2009). Both results consider radiative forcing from CO₂ only.

The dotted curve in Fig. 10 is also plotted in each of Figs 5f, 6f, 7f and 8f, for comparison with the nonlinear box model.

The second comparison in Fig. 10 is with IPCC scenario families. Because IPCC climate projections extend only to 2100, which is earlier than their time of peak temperature, we plot points ($Q(2100)$, $T(2100)$) using temperatures and their uncertainty ranges in 2100 (IPCC, 2007b) and cumulative emissions to 2100 from marker scenarios (Nakicenovic et al., 2000). For Q values less than about 2000 PgC (encompassing the B1, A1T, B2 and A1B scenarios in order of increasing Q), there is agreement to within 10% between IPCC points, the curves from eq. (8) with $R_{Np} = 0$ (dotted curve) and the median curve from Allen et al. (2009). At Q values above 2000 PgC (encompassing the A2 and A1FI scenarios), the IPCC points fall above these curves. One possible reason is that both curves describe responses to CO₂ forcing only, whereas the IPCC results include non-CO₂ forcing.

To illustrate the possible role of non-CO₂ forcing we assume that R_{Np} can be related to the CO₂ forcing quantified by Q_p . Such a relationship would be approximated if mitigation efforts were to be spread across anthropogenic greenhouse gases, so that scenarios with high cumulative future CO₂ emissions would also have high ongoing radiative forcing from non-CO₂ agents, and conversely. Because CO₂ and non-CO₂ forcings are biophysically independent, this is clearly not a general

proposition, although it is broadly consistent with detailed studies of non-CO₂ forcing (Strassmann et al., 2009, their fig. 4). A possible simple relationship between R_{Np} and Q_p , of linear form with a threshold, is

$$R_{Np} = s_N \max(0, Q_p - 500 \text{ PgC}) \quad (13)$$

where s_N [$\text{W m}^{-2} \text{PgC}^{-1}$] is the incremental non-CO₂ forcing per PgC of cumulative CO₂ emissions above 500 PgC. The threshold is consistent with the approximate present cancellation of non-CO₂ radiative forcing from gaseous and non-gaseous agents. The reference case ($R_{Np} = 0$) corresponds to $s_N = 0$.

The solid black curve in Fig. 10 shows $T_p(Q_p)$ from eq. (8), with R_{Np} described by eq. (13) with $s_N = 0.00033 \text{ W m}^{-2} \text{PgC}^{-1}$. This curve approximately matches the IPCC points, and can be regarded as the result for T_p from eq. (8) with explicit forcing from both CO₂ and non-CO₂ agents, along one line in the plane (Q_p, R_{Np}) which describes a possible association between Q_p and R_{Np} from eq. (13).

3.5. Sensitivities and uncertainties

In Fig. 11, we assess the sensitivity of $T_p(Q_p)$ (from eqs. 8 and 13) to variations in the four parameters λ_p , A_p , γ and R_{Np} (as set by s_N). Variations of λ_p and A_p are by factors (5/4, 4/5) or increments of (+25%, -20%) in each case, and variations of γ and s_N are in additive increments from zero.

First we assess the peak climate sensitivity (λ_p). The largest uncertainty in $T_p(Q_p)$ stems from uncertainty in λ_p , inherited mainly from uncertainty in the equilibrium climate sensitivity λ_q , with an additional smaller contribution from the path dependence of λ_p . Variation of λ_p in Fig. 11a by (+25%, -20%) leads to a variation in T_p of about (+1.2, -1) K at $Q_p = 2000 \text{ PgC}$, where the reference T_p is 3.1 K. The range used for λ_p is chosen to facilitate comparison with variations in A_p (for which the same proportional range is used below) and is less than the likely uncertainty inherited from λ_q , which is of order (+50%, -33%) (IPCC, 2007b). The uncertainty in $T_p(Q_p)$ resulting from uncertainty in climate sensitivity is therefore greater than the range in Fig. 11.

Secondly, the CAF at time of peak temperature (A_p) captures the response of carbon partitioning between atmospheric, terrestrial and ocean carbon reservoirs to the accumulation of anthropogenic carbon in the earth system. It is well constrained parameter because of its integral character, which causes variability in the CAF to be much less than for the instantaneous AF (see Fig. 4 and associated discussion). The present (2005–2009) CAF is 0.42, with a 5–95% uncertainty range of around $\pm 20\%$, dominated by uncertainty in cumulative emissions, mostly from cumulative land use change. Some additional uncertainty in A_p arises from path dependence (see Fig. 9 and associated discussion). A variation of A_p in Fig. 11 of (+25%, -20%) leads to a response in $T_p(Q_p)$ of about (+0.5, -0.4) K at $T_p = 2000 \text{ PgC}$.

This is less than the effect of a corresponding variation in λ_p because of the form of eq. (8), which causes T_p to respond more slowly than linearly to perturbations in A_p whereas the response to λ_p is linear.

Thirdly, the sensitivity of carbon pools to climate change (γ) accounts for effects of climate change on CO₂ fluxes, including releases of carbon from both currently mobile and currently largely immobile pools. In Fig. 11, we test additive variations in γ , taking $\gamma = 0, 40$ (reference) and 80 PgC K^{-1} , a conservative estimate of the uncertainty range (Friedlingstein et al., 2006; Sitch et al., 2008). This leads to a response in T_p which grows with Q_p below 1000 PgC, and thereafter remains nearly constant (at about +0.6 and -0.4 K for $\gamma = 80$ and 0 PgC K^{-1} , respectively) with further increase in Q_p . This behaviour stems initially from the form of eq. (8), because both the gain g and the amplification $1/(1-g)$ decrease as Q_p increases. More fundamentally, it arises from the assumption in eq. (8) of a linear response of the carbon cycle to temperature.

The temperature response of the carbon cycle is highly uncertain for two reasons: first, processes determining the effects of climate on land and ocean carbon sinks are not well understood, as reflected in the high scatter in climate responses of carbon pools in models (Friedlingstein et al., 2006, Sitch et al., 2008). Secondly, there is still poor knowledge of the vulnerability of previously undisturbed carbon pools. A major potential pool is the organic carbon in frozen soils, estimated at nearly 1700 PgC in total (Tarnocai et al., 2009), of which around 100 PgC may be vulnerable to release by thawing over the next century (Schuur et al., 2009). There is also a significant pool of carbon in tropical peatland soils, mainly in the Southeast Asian archipelago, of which around 30 PgC may be vulnerable to decomposition and fire following drainage (Hooijer et al., 2009). Net releases of carbon in other forest ecosystems are also likely through fire, insect attack and ecological transitions (Kurz et al., 2008a,b). If these uncertainties together cause the temperature response of the carbon cycle to be faster than linear, then γ would increase with increasing Q_p and T_p would increase faster with Q_p than implied by eq. (8).

Finally, we assess non-CO₂ radiative forcing at the time of peak temperature (R_{Np}). The reference value is $R_{Np} = 0$, implying no non-CO₂ forcing. Figure 11 shows the effect of parameterizing R_{Np} in eq. (8) by using eq. (13) with $s_N = 0.00033$ and $0.00066 \text{ W m}^{-2} \text{PgC}^{-1}$, corresponding respectively to an additional 0.5 and 1 W m^{-2} of radiative forcing from the aggregate of all non-CO₂ agents at $Q_p = 2000 \text{ PgC}$. These values lead respectively to increases in T_p of about 0.4 and 0.8 K at $Q_p = 2000 \text{ PgC}$, and to higher increases at larger Q_p . Non-CO₂ contributions to warming of this order are consistent with more detailed calculations of the effects of non-CO₂ forcing (Strassmann et al., 2009). The choice $s_N = 0.00033 \text{ W m}^{-2} \text{PgC}^{-1}$ approximately matches IPCC results for ($T(2100), Q(2100)$) (Fig. 10).

4. Conclusions

This paper has offered three contributions. The first is an algebraic expression (eq. 8) for $T_p(Q_p)$, the peak warming T_p associated with a cumulative total anthropogenic CO₂ emission Q_p to the time of peak warming. Given the definitions of its parameters, this expression is formally exact apart from a minor linearization with a typical error less than 1%. With reference (best-estimate) parameter values and no non-CO₂ radiative forcing, the expression is in good agreement with model results, including a non-linear box model for carbon–climate interactions (Appendix A) and also Allen et al. (2009). Equation (8) is robust for two reasons: first, it is based on a cumulative carbon budget parameterised by the CAF A_p , a conservative quantity. Second, although two of its parameters (A_p and λ_p) are path dependent, the path dependencies act in opposite ways as Q_p varies.

The second contribution is an analytic form for smooth capped emissions trajectories with a single parameter m , the long-term mitigation rate at which emissions eventually decline. This form simultaneously satisfies the requirements of a specified all-time cumulative emission, smoothness and long-term exponential decline. Its purpose here is to test eq. (8) with a non-linear box model (Appendix A), but it is likely to have other applications.

The third contribution is an assessment of vulnerabilities in the carbon–climate–human system (in the sense of risks of harm from climate change), through the lens of eq. (8). Five different vulnerabilities correspond to quantities in this equation: (1) effects of increasing CO₂ on the partition of anthropogenic carbon between atmospheric, land and ocean reservoirs (parameterised by A_p , the CAF at time t_p of peak warming); (2) effects of climate change on CO₂ fluxes (parameterized by γ , the aggregate sensitivity of land and ocean carbon to temperature change, including both currently mobile pools and currently immobile pools which are vulnerable to disturbance); (3) climate sensitivity (parameterised by λ_p , the climate sensitivity at time t_p); (4) changes in non-CO₂ radiative forcing (parameterized by R_{Np} , the net non-CO₂ forcing at time t_p); and (5) CO₂ emissions pathways (parameterized by Q_p). Two of these quantities (R_{Np} and Q_p) describe forcings by humans on the biophysical parts of the earth system, and the other three (A_p , γ and λ_p) describe biophysical processes and feedbacks. However, all contribute to vulnerability in the coupled carbon–climate–human system in the above sense.

Accounting for likely parameter variations and uncertainties, the largest vulnerability among the four parameters λ_p , A_p , γ and R_{Np} resides with λ_p , followed by R_{Np} and γ and then by A_p (Figs 10 and 11). The dominance of λ_p arises because of the high uncertainty in the equilibrium climate sensitivity λ_q , which is difficult to reduce because λ_q is strongly sensitive to small changes in positive feedbacks (Roe and Baker, 2007). However, arguably the largest vulnerability (risk of harm from climate change) in the coupled carbon–climate–human system

is that associated with Q_p , the quantity used as the primary independent variable in this analysis.

Finally, we note that eq. (8) is a conservative estimate of the relationship between cumulative emissions and peak warming because it is based on a model which cannot capture threshold crossings in the carbon–climate system. These are likely to become increasingly important at high warmings and cumulative emissions, raising the possibility that warmings and vulnerabilities are underestimated by eq. (8) at high cumulative emissions.

5. Acknowledgments

This paper is a contribution to the Global Carbon Project. MRR and JGC acknowledge with appreciation the support of the Department of Climate Change, Australian Government, which has supported the office of the Global Carbon Project in Canberra. We thank Ian Harman, John Finnigan and Ian Enting for comments on an early draft of this paper, two anonymous referees for detailed and extremely helpful comments, and Peter Briggs for assistance with figures.

Appendix A: Non-linear box model for carbon–climate system

The model state vector is

$$(C_A, C_{B1}, C_{B2}, C_{Mi}, [X]_k, \theta_j). \quad (\text{A1})$$

Its components are carbon masses [PgC] in the atmosphere (C_A), in fast and slow terrestrial biospheric C pools (C_{B1}, C_{B2}), and in a set of marine (ocean) pools (C_{Mi}); the atmospheric concentrations $[X]_k$ of non-CO₂ greenhouse gases, including CH₄, N₂O, CFC-11 and CFC-12; and global perturbation temperature components (θ_j).

A1 Atmospheric CO₂

The mass balance for atmospheric CO₂ (C_A) is

$$dC_A/dt = F_{\text{Foss}} + F_{\text{LUC}} + F_{\text{BA}} + F_{\text{MA}}, \quad (\text{A2})$$

where F_{Foss} is the anthropogenic CO₂ emission flux [PgCyr⁻¹] from fossil fuel combustion and other industrial processes including cement production, F_{LUC} is the net anthropogenic emission flux from land use change, and F_{BA} and F_{MA} are the net CO₂ fluxes to the atmosphere from the terrestrial biosphere and ocean. All fluxes are positive into the atmosphere. The atmospheric CO₂ concentration is $[CO_2]_A = C_A/r_C$, where $r_C = 2.13 \text{ PgC ppm}^{-1}$. The forcing fluxes $F_{\text{Foss}}(t)$ and $F_{\text{LUC}}(t)$ are externally prescribed, and F_{BA} and F_{MA} are specified functions of model state from phenomenological equations given in Table A1.

Table A1. Phenomenological equations for quantities in the non-linear box model

Quantity	Symbol	Phenomenological equation
Terrestrial NPP	F_{NPP} [PgC/yr]	$F_{\text{NPP}}(C_A) = F_{\text{NPP0}}(1 + \beta \ln(C_A/C_{A0}))$
Terrestrial respiration rate	k_{Bi} [y^{-1}]	$\ln(k_{Bi}) = \ln(k_{Bi(0)}) + \frac{T-T_0}{10} \ln(q_{10})$
Ocean-air CO ₂ flux	F_{MA} [PgC/yr]	$F_{\text{MA}} = k_{\text{Gas}} r_C ([\text{CO}_2]_{\text{m}} - [\text{CO}_2]_{\text{A}})$ where $[\text{CO}_2]_{\text{m}}$ and $[\text{CO}_2]_{\text{A}} = C_A/r_C$ are ocean mixed-layer and atmospheric $p\text{CO}_2$ [ppm]. $[\text{CO}_2]_{\text{m}}$ is given by (Joos et al., 1996): $[\text{CO}_2]_{\text{m}}(\text{DIC}, T) = [\text{CO}_2]_{\text{M0}} + \frac{\text{dic} \times z_a(T)}{1 - \text{dic} \times z_b(T)},$ $z_a(T) = 975.61(1.7561 - 0.031618 T + 0.0004444 T^2),$ $z_b(T) = 975.61(0.004096 - 7.7086 \times 10^{-5} T + 6.10 \times 10^{-7} T^2),$ where $\text{DIC} = \text{DIC}_0 + \text{dic}$ is the dissolved inorganic carbon [molC m^{-3}] in the ocean mixed layer, DIC_0 is its pre-industrial equilibrium value, dic is the perturbation part of DIC, and $[\text{CO}_2]_{\text{M0}} = 280$ ppm. DIC is proportional to the ocean mixed-layer carbon store [PgC], with perturbation part $c_m = \sum c_{Mi}$ given by the sum of the stores c_{Mi} determined by eq. (A5). This relationship is $\text{dic}(c_m) = (10^{15} c_m) / (A_m h_m M_C) \quad [\text{molC m}^{-3}],$ where A_m is the ocean surface area, h_m the ocean mixed-layer depth, and M_C the atomic mass of C.

Note: Notation is defined in Table A2.

A2 Terrestrial biospheric carbon

The terrestrial biospheric carbon stores C_{B1} and C_{B2} are the total carbon stores [PgC] in notional global ‘grass’ and ‘forest’ biomes, respectively (combining biomass and soil carbon, which are not separated in this model). The governing mass balance equations are

$$\begin{aligned} dC_{B1}/dt &= a_{B1} F_{\text{NPP}} - k_1 C_{B1}, \\ dC_{B2}/dt &= a_{B2} F_{\text{NPP}} - k_1 C_{B2} - F_{\text{LUC}}, \end{aligned} \quad (\text{A3})$$

where F_{NPP} is the global terrestrial net primary production (NPP) of biomass carbon [PgC y^{-1}], k_{Bi} is the turnover rate for heterotrophic respiration [y^{-1}] from biomass store i , and a_{Bi} is the fraction of global NPP entering biomass store i , with $a_{B1} + a_{B2} = 1$. The NPP is a function of $[\text{CO}_2]_{\text{A}}$ through phenomenological equations (Table A1), and the turnover rates k_{Bi} depend on the global temperature T_{A} (Table A1). The net land use change flux F_{LUC} is withdrawn from the forest carbon store C_{B2} . The biosphere-atmosphere exchange flux F_{BA} (positive into the atmosphere) is the negative terrestrial net ecosystem productivity (NEP):

$$F_{\text{BA}} = -F_{\text{NEP}} = -(F_{\text{NPP}} - k_1 C_{B1} - k_2 C_{B2}). \quad (\text{A4})$$

A3 Ocean carbon

Carbon in the ocean mixed layer (as dissolved inorganic carbon, DIC) is the sum of several stores with different turnover rates k_{Ci} for exchange with the deep ocean. The mass balances for these stores are

$$\frac{dc_{Mi}}{dt} = -a_{Ci} F_{\text{MA}} - k_{Ci} c_{Mi}; \quad c_{Mi}(0) = 0, \quad (\text{A5})$$

where $c_{Mi}(t) = C_{Mi}(t) - C_{Mi0}$ [PgC] is the perturbation of marine C store i from its pre-industrial equilibrium state C_{Mi0} , and a_{Ci} is the fraction of the atmosphere-ocean CO₂ flux entering store i (with $\sum a_{Ci} = 1$). The ocean-atmosphere flux F_{MA} (positive into the atmosphere) is a function of T_{A} and c_{Mi} (as DIC) through phenomenological equations (Table A1). Equation (A5) is equivalent to a pulse response function $\sum a_{Ci} \exp(-k_{Ci}t)$ for DIC in the ocean mixed layer (Appendix B). The weights a_{Ci} and rates k_{Ci} are specified using pulse response functions for scalar transfer from the mixed layer to the deep ocean from advanced ocean models, thus capturing the ocean dynamics represented in these models. The values of a_{Ci} and k_{Ci} used here (Table A2) are from a four-term fit to the average of the pulse response functions of the HILDA and Box-Diffusion models (Joos et al., 1996), which are in good agreement.

Table A2. Values for parameters in the nonlinear box model

Parameter	Symbol	Units	Value
Physical constants			
Mass/concentration ratios			
C in atmospheric CO ₂	r_C	PgC ppm ⁻¹	2.130
Atmospheric CH ₄	r_{CH_4}	TgCH ₄ ppb ⁻¹	2.845
Atmospheric N ₂ O	r_{N_2O}	TgN ₂ O ppb ⁻¹	7.804
Atmospheric CFC-11	r_{CFC11}	TgCFC11 ppb ⁻¹	24.36
Atmospheric CFC-12	r_{CFC12}	TgCFC12 ppb ⁻¹	21.44
Atomic mass of C	M_C	gC mol ⁻¹	12.0107
Earth radius	r_E	m	6.37×10^6
Terrestrial C parameters			
Pre-industrial terrestrial NPP	F_{NPP0}	PgC y ⁻¹	40
Parameter in NPP formulation	β		0.8
NPP partition fraction for C_{B1}	a_{B1}		0.8
Pre-industrial turnover rates:			
C_{B1} pool	$k_{B1(0)}$	yr ⁻¹	1/3
C_{B2} pool	$k_{B2(0)}$	yr ⁻¹	1/300
q_{10} for terrestrial respiration	q_{10}		2.0
Ocean C parameters			
Air-ocean gas exchange rate	k_{Gas}	yr ⁻¹	1/8.76
Ocean area	A_m	m ²	$0.7 \times 4\pi r_E^2$
Ocean mixed-layer depth	h_m	m	75
Weights in PRF for ocean CO ₂	a_{Ci}		0.512934, 0.320278, 0.142183, 0.0246045
Rates in PRF for ocean CO ₂	k_{Ci}	yr ⁻¹	5.22893, 0.356532, 0.0194692, 0.0
Pre-industrial C stores			
DIC	DIC ₀	molC m ⁻³	2.089
Global temperature	T_0	degrees C	15
Atmospheric [CO ₂]	[CO ₂] ₀	ppm	280
Atmospheric CO ₂ store	C_{A0}	PgC	$r_C [\text{CO}_2]_0$
Terrestrial C stores	$C_{Bi(0)}$	PgC	$a_{Bi} F_{NPP0} / k_{Bi(0)}$
Pre-industrial non-CO ₂ concentrations			
CH ₄	[CH ₄] ₀	ppb	700
N ₂ O	[N ₂ O] ₀	ppb	270
CFC-11, CFC-12	[CFC] ₀	ppb	0
Decay rates for non-CO ₂ gases			
CH ₄	k_{CH_4}	yr ⁻¹	$8.2^{-1} ([\text{CH}_4] / [\text{CH}_4]_0)^{-0.12}$
N ₂ O	k_{N_2O}	yr ⁻¹	1/114
CFC-11	k_{CFC11}	yr ⁻¹	1/45
CFC-12	k_{CFC12}	yr ⁻¹	1/100
Climate properties			
Weights in SRF for climate	b_{Ti}		0.434, 0.175, 0.391
Rates SRF for climate	k_{Ti}	yr ⁻¹	$4.51^{-1}, 140.4^{-1}, 1476^{-1}$
Equilibrium climate sensitivity	λ_q	K W ⁻¹ m ²	1.235
Coefficient for aerosol forcing	c_{Aero}	W m ⁻² PgC ⁻¹ y	0.12

A4 Global temperature

The absolute global temperature is $T_A(t) = T_{A0} + T(t)$, where T_{A0} is the initial (pre-industrial) temperature and $T(t)$ is the temperature perturbation. This is written as $T(t) = \sum \theta_j(t)$ [K],

with components $\theta_j(t)$ satisfying

$$\frac{d\theta_j}{dt} = k_{Tj} b_{Tj} \lambda_q R(t) - k_{Tj} \theta_j; \quad \theta_j(0) = 0 \quad (\text{A6})$$

with radiative forcing $R(t)$. The weights b_{T_j} and rates k_{T_j} characterize the climate step response function $1 - \sum b_{T_j} \exp(-k_{T_j}t)$ (Appendix B). Here we use a three-term function with coefficients (Table A2) derived by inverting the Laplace transform of the climate response function for the HadCM3 model (Li and Jarvis, 2009).

A5 Radiative forcing

Radiative forcing is taken to be the sum of contributions from anthropogenic greenhouse gases, together with aerosols:

$$R(t) = R_{\text{CO}_2}([\text{CO}_2]) + R_{\text{CH}_4}([\text{CH}_4]) + \dots + R_{\text{Aero}}. \quad (\text{A7})$$

The gases considered are CO_2 , CH_4 , N_2O and halocarbons (represented only by CFC-11 and CFC-12). We use conventional expressions for radiative forcing as a function of gas concentration (IPCC, 2001b, p. 358), specifically eq. (5) for CO_2 . The (negative) aerosol forcing is modelled as proportional to total CO_2 emissions,

$$R_{\text{Aero}}(t) = -c_{\text{Aero}}(F_{\text{Foss}}(t) + F_{\text{LUC}}(t)) \quad (\text{A8})$$

This assumes proportional relationships between aerosol radiative forcing, aerosol concentrations, aerosol emissions (taking the aerosol turnover rate to be rapid) and fossil fuel emissions. The proportionality coefficient c_{Aero} is chosen so that eq. (A7) yields a total radiative forcing of $+1.6 \text{ W m}^{-2}$ in 2005 (IPCC, 2007b). This coefficient has different units from s_N in eq. (13).

A6 Non- CO_2 greenhouse gases

Concentrations for gas X (CH_4 , N_2O or CFCs) are modelled as

$$\frac{d[X]}{dt} = r_X^{-1} (F_{X(\text{Nat})} + F_{X(\text{Anth})}(t)) - k_X[X] \quad (\text{A9})$$

with mass-concentration ratios r , fluxes F (separating natural and anthropogenic components) and atmospheric decay rates k . The assumed decay rates for N_2O and CFCs are constant, while that for CH_4 is a weak function of CH_4 concentration (Table A1) to account for the known decrease in the CH_4 decay rate from pre-industrial times to the present (Prinn, 2004). The natural fluxes $F_{(\text{Nat})}$ are taken as time-independent and set to match pre-industrial concentrations in the assumed pre-industrial equilibrium state. Past anthropogenic CH_4 fluxes are prescribed from data (Stern and Kaufmann, 1996), and past anthropogenic N_2O and CFC fluxes are prescribed as exponential functions of time. For the present illustrative calculations, future CH_4 and N_2O emissions are taken from the IPCC SRES A1B marker scenario (Nakicenovic et al., 2000) with linear extrapolation from 2100 to 2300, assuming a return to present (2000) emissions in 2300, and future halocarbon emissions are assumed constant at 2000 values.

Appendix B: Linear systems and response functions

B1 Pulse and step response functions

For a linear system with an equilibrium steady state in response to steady forcing, the forcing $f(t)$ and the response $x(t)$ (with initial condition $x(0) = 0$) are related by the alternative integral expressions

$$x(t) = \int_0^t f(\tau)g(t - \tau) d\tau, \quad (\text{B1})$$

$$x(t) = \Lambda_q \int_0^t f'(\tau)h(t - \tau) d\tau, \quad (\text{B2})$$

where $g(t)$ is the Green's function or pulse response function (PRF), $h(t)$ is the step response function (SRF), Λ_q is an equilibrium system sensitivity with the dimension of time, and a prime denotes differentiation in time ($x'(t) = dx/dt$). The PRF is the response to a unit pulse or spike forcing at $t = 0$, and the SRF is the realized fraction at time t of the equilibrium response Λ_q to a unit step forcing ($f(t) = 0$ when $t < 0$ and $f(t) = 1$ when $t \geq 0$). The relationship between the PRF and the SRF is

$$g(t) = \Lambda_q h'(t). \quad (\text{B3})$$

Requirements on $g(t)$ and $h(t)$ are $g(0) = 1$, $h(0) = 0$, and (assuming that the equilibrium state exists) $g(t) \rightarrow 0$ and $h(t) \rightarrow 1$ as $t \rightarrow \infty$. The PRF form is widely used in carbon cycle science and the SRF form in climate science, as for example in eq. (1).

B2 Systems with exponential response functions

Let the response functions $g(t)$ and $h(t)$ be sums of decaying exponential terms:

$$g(t) = \sum_i a_i \exp(-k_i t), \quad (\text{B4})$$

$$h(t) = 1 - \sum_i b_i \exp(-k_i t), \quad (\text{B5})$$

with rates k_i and weights a_i for the PRF and b_i for the SRF. These rates must sum to 1 ($\sum a_i = 1$ and $\sum b_i = 1$). The relationships between a_i and b_i are

$$b_i = \frac{a_i}{k_i \tau_q}; \quad a_i = b_i k_i \tau_q, \quad (\text{B6})$$

where τ_q is the integral time scale of the PRF,

$$\tau_q = \int_0^\infty g(\tau) d\tau = \sum_i \frac{a_i}{k_i} = \frac{1}{\sum_i b_i k_i}. \quad (\text{B7})$$

If and only if $g(t)$ and $h(t)$ respectively take the forms of eqs. (B4) and (B5), the system response $x(t)$ is a sum of terms

$x_i(t)$ which satisfy independent differential equations:

$$\frac{dx_i}{dt} = a_i f(t) - k_i x_i(t) \quad (\text{B8})$$

$$= b_i k_i \tau_q f(t) - k_i x_i(t) \quad (\text{B9})$$

with initial conditions $x_i(0) = 0$.

With steady forcing f_q , the long-term equilibrium state (denoted by a subscript q) satisfies $dx_i/dt = 0$ for all components i , so that

$$x_{qi} = \frac{a_i f_q}{k_i}; \quad x_q = \sum_i x_{qi} = \tau_q f_q. \quad (\text{B10})$$

B3 System sensitivity

A measure of the sensitivity of the system at time t is the instantaneous ratio of response to forcing, $\Lambda(t) = x(t)/f(t)$, with the dimension of time. The long-term equilibrium sensitivity with steady forcing f_q is $\Lambda_q = x_q/f_q$ (eq. B2). eq. (B10) yields two forms for Λ_q :

$$\Lambda_q = \tau_q \quad \text{and} \quad \Lambda_q = \frac{\sum_i x_{qi}}{\sum_i k_i x_{qi}}. \quad (\text{B11})$$

Assuming the solution $x(t)$ has a peak value (more generally, a local extremum) at time t_p , we can also find the peak sensitivity $\Lambda_p = x_p/f_p$, where $x_p = x(t_p)$ and $f_p = f(t_p)$. At the time t_p we have $dx/dt = \sum dx_i/dt = 0$. Summing eq. (B8) over i and equating to zero, this yields

$$\Lambda_p = \frac{\sum_i x_{pi}}{\sum_i k_i x_{pi}}. \quad (\text{B12})$$

Eqs. (B11) and (B12) show that the sensitivities Λ at long-term equilibrium and at the peak time t_p are both given by weighted parallel averages of the component time scales k_i^{-1} , where the weights are the component stores x_i at the relevant times. In both cases, this is true because of the constraint $\sum dx_i/dt = 0$. At long-term equilibrium, but not at the peak time t_p , the system also satisfies the stronger constraint $dx_i/dt = 0$ for each component i . For systems with a finite τ_q the equilibrium sensitivity Λ_q is path-independent, but the peak sensitivity Λ_p depends on the forcing path $f(t)$ which yields the peak x_p .

B4 Response functions and sensitivities for global temperature

For global temperature, the SRF expression is eq. (1). Also writing the PRF form using eq. (B1), this is

$$T(t) = \frac{1}{H} \int_0^t R(\tau) g_T(t - \tau) d\tau \quad (\text{B13})$$

$$= \lambda_q \int_0^t R'(\tau) h_T(t - \tau) d\tau, \quad (\text{B14})$$

where $T(t)$ is the global temperature perturbation [K], $R(t)$ is the radiative forcing [W m^{-2}], H is an average heat capacity for the thermal stores which interact with climate [$\text{J m}^{-2} \text{K}^{-1}$], $g_T(t)$ and $h_T(t)$ are respectively the PRF and SRF for climate, and λ_q is the equilibrium climate sensitivity [$\text{K W}^{-1} \text{m}^2$]. The equilibrium and peak climate sensitivities λ_q and λ_p are related to H and the response function by

$$\lambda_q = \Lambda_q/H = \tau_q/H; \quad \lambda_p = \Lambda_p/H, \quad (\text{B15})$$

where Λ_q and Λ_p are sensitivities with the dimension of time given by eqs. (B11) and (B12), and τ_q is given by eq. (B7) in terms of coefficients in an exponential response function.

Appendix C: Data sources

Data on past CO_2 emissions from fossil fuels and other industrial processes (mainly cement production) are from the Carbon Dioxide Information and Analysis Center (CDIAC), US Department of Energy (Boden et al., 2009).

Data on past CO_2 emissions from land use change are from Houghton (2003), updated by the Global Carbon Project (Le Quere et al., 2009).

Data for CO_2 concentrations are the average of annual-mean concentrations at Mauna Loa and the South Pole, from the Scripps Institution of Oceanography (Keeling et al., 2001, 2005).

Temperature data are annual global temperatures from the Climatic Research Unit, University of East Anglia (<http://www.cru.uea.ac.uk/cru/data/temperature/>).

Annual time series for the AF and CAF were inferred from the above data on CO_2 emissions and concentrations, using the definitions of the AF and CAF (Raupach et al., 2008).

References

- Allen, M. R., Frame, D. J., Huntingford, C., Jones, C. D., Lowe, J. A. and co-authors. 2009. Warming caused by cumulative carbon emissions: towards the trillionth tonne. *Nature* **458**, 1163–1166.
- Boden, T. A., Marland, G. and Andres, R. J. 2009. *Global, Regional, and National Fossil-Fuel CO_2 Emissions*, Carbon Dioxide Information Analysis Center, Oak Ridge National Laboratory, U.S. Department of Energy, Oak Ridge, TN, USA.
- Canadell, J. G., Le Quere, C., Raupach, M. R., Field, C. B., Buitenhuis E. T. and co-authors. 2007. Contributions to accelerating atmospheric CO_2 growth from economic activity, carbon intensity, and efficiency of natural sinks. *Proc. Natl. Acad. Sci. USA* **104**, 18866–18870.
- Cox, P. M., Betts, R. A., Jones, C. D., Spall, S. A. and Totterdell, I. J. 2000. Acceleration of global warming due to carbon-cycle feedbacks in a coupled climate model. *Nature* **408**, 184–187.
- Den Elzen, M. G. J., Berk, M., Schaeffer, M., Olivier, J. G. J., Hendriks, C. and Metz, B. 1999. The Brazilian proposal and other options for international burden sharing: an evaluation of methodological and policy aspects using the FAIR model. Report No. 72801011, National Institute of Public Health and the Environment, Bilthoven, The Netherlands.

- Frame, D. J., Stone, D. A., Stott, P. A. and Allen, M. R. 2006. Alternatives to stabilization scenarios. *Geophys. Res. Lett.* **33**, doi:10.1029/2006GL025801.
- Friedlingstein, P., Cox, P., Betts, R., Bopp, L., von Bloh, W. and co-authors. 2006. Climate-carbon cycle feedback analysis: results from the C4MIP model intercomparison. *J. Clim.* **19**, 3337–3353.
- Gruber, N., Friedlingstein, P., Field, C. B., Valentini, R., Heimann, M. and co-authors. 2004. The vulnerability of the carbon cycle in the 21st century: an assessment of carbon-climate-human interactions. In: *The Global Carbon Cycle: Integrating Humans, Climate, and the Natural World*, (eds. C. B. Field and M. R. Raupach), Island Press, Washington, 45–76.
- Hansen, J. E., Sato, M., Kharecha, P., Beerling, D. J., Masson-Delmotte V. and co-authors. 2008. Target atmospheric CO₂: where should humanity aim?. *Open Atmos. Sci. J.* **2**, 217–231.
- Hooijer, A., Page, S., Canadell, J. G., Silvius, M., Kwadijk, J. and co-authors. 2009. Current and future CO₂ emissions from drained peatlands in Southeast Asia. *Biogeosci. Discuss.* **6**, 7207–7230.
- Houghton, R. A. 2003. Revised estimates of the annual net flux of carbon to the atmosphere from changes in land use and land management 1850–2000. *Tellus* **55B**, 378–390.
- IPCC 2001a. Climate Change 2001: Impacts, Adaptation, and Vulnerability. Contribution of Working Group II to the Third Assessment Report of the Intergovernmental Panel on Climate Change, Cambridge University Press, Cambridge, UK.
- IPCC 2001b. Climate Change 2001: The Scientific Basis. Contribution of Working Group I to the Third Assessment Report of the Intergovernmental Panel on Climate Change, Cambridge University Press, Cambridge, United Kingdom and New York.
- IPCC 2007a. Climate Change 2007: Impacts, Adaptation and Vulnerability. Contribution of Working Group II to the Fourth Assessment Report of the Intergovernmental Panel on Climate Change. Cambridge University Press, Cambridge, UK and New York, NY, USA, 976 pp.
- IPCC 2007b. Climate Change 2007: The Physical Science Basis. Contribution of Working Group I to the Fourth Assessment Report of the Intergovernmental Panel on Climate Change. Cambridge University Press, Cambridge, UK and New York, NY, USA, 996 pp.
- Joos, F., Bruno, M., Fink, R., Siegenthaler, U., Stocker, T. F. and co-authors. 1996. An efficient and accurate representation of complex oceanic and biospheric models of anthropogenic carbon uptake. *Tellus Series B-Chem. Phys. Meteorol.* **48**, 397–417.
- Keeling, C. D., Piper, S. C., Bacastow, R. B., Wahlen, M., Whorf, T. P. and co-authors. 2001. Exchanges of atmospheric CO₂ and ¹³CO₂ with the terrestrial biosphere and oceans from 1978 to 2000. *I. Global Aspects*, SIO Reference Series, No. 01-06, Scripps Institution of Oceanography, San Diego.
- Keeling, C. D., Piper, S. C., Bacastow, R. B., Wahlen, M., Whorf, T. P. and co-authors. 2005. Atmospheric CO₂ and ¹³CO₂ exchange with the terrestrial biosphere and oceans from 1978 to 2000: observations and carbon cycle implications. In: *A History of Atmospheric CO₂ and its effects on Plants, Animals, and Ecosystems*, (eds. J. R. Ehleringer, T. E. Cerling and M. D. Dearing), Springer Verlag, New York, 83–113.
- Knutti, R. and Hegerl, G. C. 2008. The equilibrium sensitivity of the Earth's temperature to radiation changes. *Nat. Geosci.* **1**, 735–743.
- Kurz, W. A., Dymond, C. C., Stinson, G., Rampley, G. J., Neilson, E. T. and co-authors. 2008a. Mountain pine beetle and forest carbon feedback to climate change. *Nature* **452**, 987–990.
- Kurz, W. A., Stinson, G., Rampley, G. J., Dymond, C. C. and Neilson, E. T. 2008b. Risk of natural disturbances makes future contribution of Canada's forests to the global carbon cycle highly uncertain. *Proc. Natl. Acad. Sci. USA* **105**, 1551–1555.
- Le Quere, C., Raupach, M. R., Canadell, J. G., Marland, G., Bopp, L. and co-authors. 2009. Trends in the sources and sinks of carbon dioxide. *Nat. Geosci.* **2**, doi:10.1038/NGEO689.
- Li, S. and Jarvis, A. 2009. Long run surface temperature dynamics of an A-OGCM: the HadCM3 4xCO₂ forcing experiment revisited. *Clim. Dyn.* **33**, 817–825.
- Li, S., Jarvis, A. J. and Leedal, D. T. 2009. Are response function representations of the global carbon cycle ever interpretable? *Tellus* **61B**, 361–371.
- Lowe, J. A., Huntingford, C., Raper, S. C. B., Jones, C. D., Liddicoat, S. K. and co-authors. 2009. How difficult is it to recover from dangerous levels of global warming? *Environ. Res. Lett.* **4**, doi:10.1088/1748-9326/4/1/014012.
- Matthews, H. D., Gillett, N. P., Stott, P. A. and Zickfeld, K. 2009. The proportionality of global warming to cumulative carbon emissions. *Nature* **459**, 829–833.
- Meinshausen, M. 2006. What does a 2C target mean for greenhouse gas concentrations? A brief analysis based on multi-gas emission pathways and several climate sensitivity uncertainty estimates. In: *Avoiding Dangerous Climate Change*, (eds. H. J. Schellnhuber, W. Cramer, N. Nakicenovic, T. M. L. Wigley and G. Yohe), Cambridge University Press, Cambridge, 265–279.
- Meinshausen, M., Meinshausen, N., Hare, W., Raper, S. C. B., Frieler, K. and co-authors. 2009. Greenhouse gas emission targets for limiting global warming to 2°C. *Nature* **458**, 1158–1162.
- Myhre, G., Highwood, E. J., Shine, K. P. and Stordal, F. 1998. New estimates of radiative forcing due to well mixed greenhouse gases. *Geophys. Res. Lett.* **25**, 2715–2718.
- Nakicenovic, N., Alcamo, J., Davis, G., de Vries, B., Fenhann, J. and co-authors. 2000. IPCC Special Report on Emissions Scenarios. Cambridge University Press, Cambridge, U.K. and New York, 599 pp.
- Oeschger, H., Siegenthaler, U., Schotterer, U. and Gugelmann, A. 1975. Box diffusion-model to study carbon-dioxide exchange in nature. *Tellus* **27**, 168–192.
- Prinn, R. G. 2004. Non-CO₂ greenhouse gases. In: *The Global Carbon Cycle: Integrating Humans, Climate, and the Natural World*, (eds. C. B. Field and M. R. Raupach), Island Press, Washington, 205–216.
- Ramanathan, V. and Feng, Y. 2008. On avoiding dangerous anthropogenic interference with the climate system: formidable challenges ahead. *Proc. Natl. Acad. Sci. USA* **105**, 14245–14250.
- Raupach, M. R. and Canadell, J. G. 2010. Carbon and the anthropocene. *Curr. Opin. Environ. Sustainabil.* **4**, doi:10.1016/j.cosust.2010.04.003.
- Raupach, M. R., Canadell, J. G. and Le Quere, C. 2008. Anthropogenic and biophysical contributions to increasing atmospheric CO₂ growth rate and airborne fraction. *Biogeosciences* **5**, 1601–1613.
- Raupach, M. R., Marland, G., Ciais, P., Le Quere, C., Canadell, J. G. and co-authors. 2007. Global and regional drivers of accelerating CO₂ emissions. *Proc. Natl. Acad. Sci. USA* **104**, 10288–10293.

- Roe, G. H. and Baker, M. B. 2007. Why is climate sensitivity so unpredictable? *Science* **318**, 629–632.
- Schellnhuber, H. J., Cramer, W., Nakicenovic, N., Wigley, T. M. L. and Yohe, G. 2006. *Avoiding Dangerous Climate Change*. Cambridge University Press, Cambridge, 392 pp.
- Schuur, E. A. G., Bockheim, J., Canadell, J. G., Euskirchen, E., Field, C. B. and co-authors. 2008. Vulnerability of permafrost carbon to climate change: implications for the global carbon cycle. *BioScience* **58**, 701–714.
- Schuur, E. A. G., Vogel, J. G., Crummer, K. G., Lee, H., Sickman, J. O. and co-authors. 2009. The effect of permafrost thaw on old carbon release and net carbon exchange from tundra. *Nature* **459**, 556–559.
- Sitch, S., Huntingford, C., Gedney, N., Levy, P. E., Lomas, M. and co-authors. 2008. Evaluation of the terrestrial carbon cycle, future plant geography and climate-carbon cycle feedbacks using five Dynamic Global Vegetation Models (DGVMs). *Global Change Biol.* **14**, 2015–2039.
- Solomon, S., Plattner, G. K., Knutti, R. and Friedlingstein, P. 2009. Irreversible climate change due to carbon dioxide emissions. *Proc. Natl. Acad. Sci. USA* **106**, 1704–1709.
- Steffen, W. L., Sanderson, A., Tyson, P. D., Jager, J., Matson, P. A. and co-authors. 2004. *Global Change and the Earth System: A Planet Under Pressure*. Springer, Berlin, 336 pp.
- Stern, D. I. and Kaufmann, R. K. 1996. Estimates of global anthropogenic methane emissions 1860–1993. *Chemosphere* **33**, 159–176.
- Strassmann, K. M., Plattner, G. K. and Joos, F. 2009. CO₂ and non-CO₂ radiative forcings in climate projections for twenty-first century mitigation scenarios. *Clim. Dyn.* **33**, 737–749.
- Tarnocai, C., Canadell, J. G., Schuur, E. A. G., Kuhry, P., Mazhitova, G. and co-authors. 2009. Soil organic carbon pools in the northern circumpolar permafrost region. *Glob. Biogeochem. Cycles* **23**, GB2023, doi:10.1029/2008GB003327.
- Trudinger, C. M. and Enting, I. G. 2005. Comparison of formalisms for attributing responsibility for climate change: Non-linearities in the Brazilian proposal approach. *Clim. Change* **68**, 67–99.
- Turner, B. L., Kasperson, R. E., Matson, P. A., McCarthy, J. J., Corell, R. W. and co-authors. 2003. A framework for vulnerability analysis in sustainability science. *Proc. Natl. Acad. Sci. USA* **100**, 8074–8079.
- Zickfeld, K., Eby, M., Matthews, H. D. and Weaver, A. J. 2009. Setting cumulative emissions targets to reduce the risk of dangerous climate change. *Proc. Natl. Acad. Sci. USA* **106**, 16129–16134.
- Zimov, S. A., Schuur, E. A. G. and Chapin, F. S. 2006. Permafrost and the global carbon budget. *Science* **312**, 1612–1613.